LJMU Research Online

Banerjee, S, Phuneerub, P, Jaidee, W, Rujanapun, N, Duangyod, T, Malee, K, Maneerat, W, Suthiphasilp, V, Laphookhieo, S, Ramli, S, Mah, SH, Chansukh, KK, Hiransai, P, Puttarak, P, Sarker, SD, Nahar, L and Charoensup, R

 Abutilon indicum (L.) Sweet Extracts Inhibit Key Glucose Metabolic Enzymes While Enhancing Glucose Transport in L6 Myotubes and 3T3L1 Adipocytes

https://researchonline.ljmu.ac.uk/id/eprint/27320/

Article

WILEY

Research Article

Abutilon indicum (L.) Sweet Extracts Inhibit Key Glucose Metabolic Enzymes While Enhancing Glucose Transport in L6 Myotubes and 3T3L1 Adipocytes

Subhadip Banerjee [1], **Pravaree Phuneerub** [1,2] **Wuttichai Jaidee** [2]
Narawadee Rujanapun [1], **Thidarat Duangyod** [1,2] **Kulwadee Malee** [1]
Wisanu Maneerat [1,3] **Virayu Suthiphasilp** [4], **Surat Laphookhieo** [1,3]
Salfarina Ramli [5], **Siau Hui Mah** [6] **Kitthisak Khlaeo Chansukh** [7]
Poonsit Hiransai [8,9] **Panupong Puttarak** [10,11] **Satyajit D. Sarker** [12] **Lutfun Nahar** [13]
and **Rawiwan Charoensup** [1,2]

[1]*Medicinal Plant Innovation Center, Mae Fah Luang University, Chiang Rai 57100, Thailand*
[2]*School of Integrative Medicine, Mae Fah Luang University, Chiang Rai 57100, Thailand*
[3]*Center of Chemical Innovation for Sustainability (CIS), School of Science, Mae Fah Luang University, Chiang Rai 57100, Thailand*
[4]*Department of Industrial Technology and Innovation Management, Faculty of Science and Technology, Pathumwan Institute of Technology, Bangkok 10330, Thailand*
[5]*Faculty of Pharmacy, Universiti Teknologi MARA Cawangan Selangor, Puncak Alam 42300, Selangor, Malaysia*
[6]*School of Biosciences, Faculty of Health and Medical Sciences, Taylor's University, Subang Jaya 47500, Selangor, Malaysia*
[7]*Department of Applied Thai Traditional Medicine, College of Allied Health Sciences, Suan Sunandha Rajabhat University, Bangkok 10300, Thailand*
[8]*Department of Medical Technology, School of Allied Health Sciences, Walailak University, Nakhon Si Thammarat 80160, Thailand*
[9]*Herbology Research Center, Walailak University, Nakhon Si Thammarat 80160, Thailand*
[10]*Phytomedicine and Pharmaceutical Biotechnology Excellence Center, Faculty of Pharmaceutical Sciences, Prince of Songkla University, Songkhla 90110, Thailand*
[11]*Department of Pharmacognosy and Pharmaceutical Botany, Faculty of Pharmaceutical Sciences, Prince of Songkla University, Songkhla 90110, Thailand*
[12]*Centre for Natural Products Discovery, School of Pharmacy and Biomolecular Sciences, Liverpool John Moores University, Liverpool L3 3AF, UK*
[13]*Laboratory of Growth Regulators, Palacký University and Institute of Experimental Botany, The Czech Academy of Sciences, Olomouc 78371, Czech Republic*

Correspondence should be addressed to Rawiwan Charoensup; rawiwan.cha@mfu.ac.th

Background: *Abutilon indicum* (L.) Sweet (Malvaceae) is a traditional medicinal plant known for its antidiabetic properties in Ayurveda and other health systems.
Aims: This study aims to profile metabolites in *Abutilon indicum* (L.) Sweet extracts (AI) and elucidate their antidiabetic mechanisms through bioinformatics and experimental methods.
Study Design: The ethanolic (AIE) and aqueous (AIA) extracts were evaluated for their inhibitory effects on α-glucosidase and α-amylase, as well as their impact on glucose metabolism in 3T3-L1 adipocytes and L6 skeletal muscle cells. AIE was characterized via HPLC-DAD-QTOF-MS, with network pharmacology and molecular docking analyses used to explore molecular targets.

Methods: In vitro assays were performed to assess enzyme inhibition, and cell line studies HPLC-DAD-QTOF-MS were utilized for compound characterization. Network pharmacology and molecular docking were conducted to reveal underlying antidiabetic mechanisms.

Results: LC-MS-QTOF analysis identified gallic acid, stigmasterol, and riboflavin as abundant compounds. The AIE exhibited significant α-glucosidase ($IC_{50} = 74.15 \pm 1.61\ \mu g/mL$) and α-amylase inhibition ($IC_{50} = 13.41 \pm 0.71\ \mu g/mL$). Moreover, it enhanced glucose consumption in 3T3-L1 cells ($IC_{50} = 6.25\ \mu g/mL$) and promoted glucose uptake in L6 myotubes. Network pharmacology analyses highlighted the PI3K–Akt signaling pathway's role in facilitating glucose transport.

Conclusion: The phytochemicals in AIE may contribute significantly to its antidiabetic effects, particularly through the modulation of glucose transport via the PI3K–Akt pathway. Future studies should focus on the preclinical development of safe herbal formulations utilizing these mechanisms for effective diabetes management.

Keywords: *Abutilon indicum*; antidiabetic activity; glucose transport; LC-MS-QTOF; network pharmacology

1. Introduction

Diabetes is a chronic metabolic disorder characterized by insufficient insulin production or insulin resistance. This condition is influenced by various factors, including genetics and environmental circumstances [1]. Diabetic medications, metformin, SGLT2 inhibitors, and GLP1 receptor agonists, reduce blood sugar levels with significant side effects. DPP4 inhibitors are regarded as safer alternatives, particularly for individuals vulnerable to such complications [2, 3]. The potential side effects of diabetes medications highlight the importance of preventive measures aimed at reducing the risk of developing diabetes.

Herbal medicines are receiving attention because they provide multi-targeted compounds that can affect multiple pathways involved in diabetes. These natural ingredients can enhance insulin sensitivity, promote glucose uptake, and lower blood sugar levels [4]. Ayurveda, the traditional Indian system of medicine, offers various methods for managing complex metabolic diseases like diabetes, including herbal treatments and dietary guidance [5, 6]. Some studies also reported on the in vitro bioactivity and metabolite profiles of herbal combinations, suggesting their potential in diabetes management [7].

Abutilon indicum (L.) Sweet commonly known as Indian mallow or "Aatibala" is a notable medicinal plant used in Ayurveda. Its antidiabetic properties come from various bioactive compounds, including abutilin A, alkaloids, flavonoids, polysaccharides, and phenolic compounds present in the extract [8]. The antidiabetic potential of *Abutilon indicum* has been extensively studied in previous research, highlighting its mechanisms of action, bioactive compounds, and pharmacological effects.

Recent advancements in network pharmacology and high-resolution techniques like LC-MS/MS have deepened insights into the molecular mechanisms of traditional medicinal plants [9, 10]. Network pharmacology leverages multi-omics data to systemically evaluate drug–response interactions [11], while LC-MS/MS enables the precise chemical profiling of herbal extracts, critical for identifying multi-component therapeutics. Integrating these approaches, particularly with LC-MS-QTOF, clarifies the poly-pharmacological effects of traditional herbal mixtures by mapping interactions among phytochemicals, disease targets, and molecular networks [5, 6, 10, 12, 13]. Such strategies elucidate synergistic mechanisms and systemic therapeutic benefits, advancing the study of herbal medicine [9].

Previous research has extensively documented the antidiabetic potential of *A. indicum*, with studies highlighting its capacity to modulate glucose metabolism through enzyme inhibition. Methanolic leaf extracts of *A. indicum* were shown to suppress the α-glucosidase activity in both normal and diabetic rats [14], aligning with the enzymatic inhibition observed in the current study. Significant in vitro α-amylase and α-glucosidase inhibitory effects of root extracts were also reported [15], further corroborating this mechanism. Beyond enzyme modulation, aqueous extracts of *A. indicum* were found to enhance glucose homeostasis by inhibiting intestinal glucose absorption and stimulating insulin secretion [16, 17], while its in vitro efficacy among other medicinal plants was confirmed [17]. The present study extends these insights by employing network pharmacology and molecular docking to elucidate systemic interactions between *A. indicum* compounds and diabetes-related molecular targets, a novel approach not previously explored. Phytochemical analyses identified bioactive markers such as gallic acid and quercetin [8, 18], which this work reinforces through the HPLC-DAD-QTOF-MS characterization of extract constituents, underscoring their antidiabetic and antioxidant roles. Additionally, antioxidant and anti-inflammatory properties linked to oxidative stress mitigation and β-cell protection were documented [19–23], supporting the current findings. Collectively, this study integrates multifaceted methodologies to advance the mechanistic understanding of *A. indicum* in diabetes management, bridging traditional pharmacological assessments with contemporary computational and analytical techniques.

In this study, the ethanolic extract of *A. indicum* (AIE) and the aqueous extract (AIA) were evaluated for their in vitro inhibitory effects on α-glucosidase and α-amylase enzymes. The influence of these extracts on glucose consumption, uptake, and cell viability was also examined in 3T3-L1 adipocytes and L6 skeletal muscle cells. The characterization of AIE was performed using HPLC-DAD-QTOF-MS, while network pharmacology and molecular docking analyses were conducted to clarify the molecular mechanisms behind the observed bioactivities. One notable

distinction of this study is its evaluation of glucose consumption, uptake, and cell viability in 3T3-L1 adipocytes and L6 skeletal muscle cells, which was not extensively explored in previous research. Additionally, while past studies primarily focused on crude extracts, this study provides a more comprehensive system-level pharmacological analysis of *A. indicum* using network pharmacology and LC-MS/MS profiling. This approach enhances our understanding of the plant's poly-pharmacological effects, setting this study apart by bridging traditional knowledge with advanced molecular techniques.

2. Materials and Methods

2.1. Materials and Instruments. Methanol (Analytical Reagent grade, CAS No. 67-56-1), formic acid (HPLC grade, CAS No. 64-18-6), and acetonitrile (HPLC grade, CAS No. 67-64-1) were obtained from Fisher Scientific in the United Kingdom. Additional chemicals and reagents were sourced from ACROS Organics or Sigma-Aldrich in the USA. The mobile phase for the analyses was filtered using membrane filters from Millipore, featuring a pore size of 0.45 μm. In addition, samples underwent filtration using Millipak Express syringe filters, which also have a pore size of 0.45 μm. Necessary equipment included a rotary vacuum evaporator from Buchi, Germany, and an Agilent 6500 Series LC Q-TOF System equipped with an electrospray ionization (ESI) interface for high-resolution mass spectrometry analysis.

2.2. Plant Extract Preparation. The aerial parts of *Abutilon indicum* were obtained from Ayurawet Wattana Medicine Limited Partnership in Thailand and were carefully stored at room temperature, around 27°C–30°C. A specimen of the plant with voucher number MPIC/MT/22/05 was deposited at the Medicinal Plant Innovation Centre at Mae Fah Luang University, located in Chiang Rai, Thailand. The collected plant material was thoroughly washed under running water to remove any impurities, followed by shade drying to retain its properties. Once dried, the plant material was ground into a fine powder using an electronic mixer grinder. The weights recorded for the raw and powdered plant materials were approximately 700 g and 500 g, respectively.

The ethanolic (AIE) and aqueous (AIA) extracts were prepared by extracting the powder with ethanol (3 × 500 mL) and distilled water (3 × 1 L), respectively, at room temperature for 48 h with occasional shaking. Following the extraction processes for both methods, the mixtures were filtered to separate the liquid extracts from the solid plant material. The resulting extracts were then evaporated to dryness under reduced pressure using a rotary vacuum evaporator and subsequently freeze-dried to obtain a concentrated form of the extracts.

2.3. Pharmacological Activity

2.3.1. α-Glucosidase Inhibition Activity. The activity of the α-glucosidase inhibition was conducted following the procedure described in the literature with some modifications [7]. The inhibitory effect of AI extracts was evaluated at various concentrations (5, 10, 20, 35, 50, 75, and 100 μg/mL). Each extract (50 μL) was mixed with 0.35 U/mL α-of glucosidase solution (100 μL) and incubated at 37°C for 10 min. Subsequently, 1.5 mM of *p*-NPG solution (100 μL) was added and incubated again at 37°C for 20 min. The reaction was terminated by adding sodium carbonate (1000 μL) solution. After stopping the reaction, the absorbance of the resulting solution was measured at a wavelength of 405 nm using a microplate reader. Acarbose, a well-known α-glucosidase inhibitor, was used as a positive control for comparison.

2.3.2. α-Amylase Inhibition Activity. The α-amylase inhibitory activity of the AI extracts was measured with minor modifications following the literature [20, 24] with some modification. A starch solution was prepared (120 μL), and the plant extracts AIE and AIA (60 μL) at various concentrations (5, 10, 20, 35, 50, 75, and 100 μg/mL) were prepared. This mixture was then incubated at 37°C for 10 min. After incubation, 1 U/mL of α-amylase solution (180 μL) was added to the mixture, which was subsequently incubated for an additional 30 min. The reaction was stopped by adding 0.1 M hydrochloric acid solution (1 mL) followed by 1 mM iodine solution (100 μL). The absorbance of the solution was measured at a wavelength of 650 nm using a microplate reader (EnVision, Perkin Elmer, Waltham, MA). Acarbose was again utilized as a positive control for the experiments.

2.3.3. Glucose Diffusion Retardation Assay. The glucose diffusion retardation assay was adapted from a method described in the literature to examine the effect of the extracts on glucose diffusion [25]. A one-sided sealed dialysis tube was utilized for this experiment. The tube was filled with 22 mM D-glucose (1 mL) in 0.15 M NaCl (1 mL), and then AI extracts were added to the tube at various concentrations (25, 12.5, and 6.25 mg/mL). After filling the tube, the other end of the tube was sealed, and the dialysis membrane was submerged in a conical flask that contained 0.15 M NaCl (45 mL). The effects of the extracts on glucose diffusion were observed and recorded at intervals of 2, 4, and 6 h. An aliquot (10 μL) of the external solution was withdrawn at each interval and tested for the presence of glucose, using a glucose oxidase kit (Biosystems, Spain). A standard curve was constructed using different glucose concentrations. The glucose diffusion retardation index (GDRI) was calculated using the following formula below, and all experiments were carried out in triplicate to ensure the reliability of the results

$$GDRI = \left(\frac{100 - \text{glucose content (mg/mL) in external solution in the presence of plant extract}}{\text{glucose content (mg/mL) in external solution in the absence of plant extract}} \right) \times 100. \tag{1}$$

2.4. Experimental Validation of the Antidiabetic Potential of AI Extracts in Adipocytes and Skeletal Muscle. The antidiabetic potential of AI extracts was evaluated using 3T3 preadipocyte cells (ATCC, Manassas, VA, USA, Catalog No. CL-173, CVCL_0123). The cells were grown for 24 h in DMEM (Dulbecco's modified Eagle's medium) culture media that contained 10% (v/v) fetal bovine serum (FBS), 100 U/L of penicillin, 100 U/L of streptomycin, 2 mM of glutamine, and glucose solution (3 mg/mL). The incubation atmosphere was maintained at a temperature of 37°C with 5% CO_2. Cells were treated with AI extracts for 24 h in DMEM containing 4 mg/mL of glucose. After 24 h, 10 µL of the supernatant was used to measure glucose consumption using the glucose oxidase–peroxidase assay, with glucose levels quantified using a standard curve ranging from 0.5 to 4 mg/mL. The percent of glucose consumption was calculated using the following formula and IC50 was determined

$$\text{Glucose consumption} = \frac{(A - B)}{(A - C)} \times 100, \qquad (2)$$

$A =$ Glucose concentration in the control medium. $B =$ Glucose concentration in the sample medium. $C =$ Blank control without cell in the medium.

L6 myotubes (ATCC, Manassas, VA, USA, Catalog No. CRL-1458, CVCL_0385) were grown in DMEM with 10% (v/v) FBS, along with 100 U/L of penicillin and 100 U/L of streptomycin. These myotubes were incubated in a humidified environment consisting of 95% air and 5% CO_2 at 37°C for 24 h. After the initial culture, the cells were reseeded at a density of 2×10^4 cells/mL in either 6-well plates or 24-well plates for subsequent glucose uptake assays. Once the cells attained approximately 80% confluence, the medium was switched to DMEM supplemented with a reduced concentration of 2% (v/v) FBS. This media change occurred after 24 h and was repeated at intervals of 2, 4, and 6 days to provide optimal growth conditions. When myotube differentiation was completed on day 7, the experiment commenced.

L6 myotubes were treated with AI extracts and metformin, which was used as a positive control, for a duration of 24 h. After treatment, the cells were subjected to 80 µM of 2-NBDG for 60 min after being rinsed twice with Krebs Ringer bicarbonate buffer to determine glucose uptake. The fluorescence intensity of the samples was measured at excitation/emission wavelengths of 485/530 nm using a microplate reader (EnVision, Perkin Elmer, Waltham, MA). This measurement provided insights into the glucose uptake capabilities of the myotubes in response to the treatments.

2.5. Liquid Chromatography–Mass Spectrometer (LC/QTOF-MS) Analysis. The AIE (1 mg) was dissolved in LC/MS grade methanol (1 mL) and then filtered through a PTFE membrane syringe filter (0.22 µm). The chemical analysis of AIE was conducted using a liquid chromatography/time-of-flight mass spectrometer (Agilent 6500 Series LC Q-TOF System) equipped with a dual ASI ESI interface. Chromatographic separation was accomplished with an Agilent LC-QTOF 6500 system utilizing an Agilent ZORBAX Eclipse Plus—C_{18} column (2.1×50 mm, 1.8 µm). The mobile phase consisted of water containing 0.1% formic acid (A) and acetonitrile (0.1% formic acid) (B) at a flow rate of 200 µL/min. The injection volume was 1 µL. The column temperature was maintained at 25°C throughout the analysis.

The MS1 acquisition was set with a minimum range (m/z) of 103 and a maximum range (m/z) of 1100 with a scan rate (spectra/sec) of 1.00. The detection window was established at 100 ppm. The flow rate was maintained at 1 mL/min, starting with 5% mobile phase B for 1 min and increasing linearly to 17% B in 13 min. The flow was then increased to 100% mobile phase B within 22 min, and the eluent composition was held steady for 2 min before being reduced back to 5% mobile phase B over the same 2 min, applying both positive and negative ion modes. The nebulizer pressure was set at 45 psi. The MS/MS absolute threshold was established at five per peak.

The identification of compounds was performed utilizing Agilent Mass Hunter B.08.00 software (Qualitative navigator, Qualitative workflows) along with the PCDL database. The height of the peaks at 10,000 in both profile and centroid spectra indicated significance, with a relative peak height of 0.1% compared to the highest peak. An algorithm was used to determine a quality score greater than 70%, which assessed the reliability of the detected feature as a compound. The following factors included the signal-to-noise ratio, retention time peak shape, retention time peak width, consistency of ion retention time, mass differences between ion species, and the isotope pattern when setting the quality score. The identification of peaks was achieved by comparing retention time, mass spectra, and fragmentation patterns with reference compounds from the library, using the PCDL database (including the TCM database, phenolic acid database, and PubChem chemical database), while maintaining high accuracy (error < 5 ppm). MS/MS matching of major fragments was utilized for further confirmation. Mass tolerances were established with the precursor ion at ± 10 ppm and the fragment ion at ± 15 ppm. The unit mass tolerance was set at 0.3 Da, with an abundance ratio of 40%.

2.6. Target Search and ADME Profiling. The GEO database was searched for suitable datasets, leading to the selection of GSE81965 (https://www.ncbi.nlm.nih.gov/geo/query/acc.cgi?acc=GSE81965), which was loaded into the Biojupies notebook. The expression data were quantified as gene-level counts using the ARCHS pipeline. The data normalization was performed by converting the raw counts to log10-counts per million (logCPM). The gene expression signature was generated by comparing gene expression levels between the control group and the experimental group using the Limma R package. The high-dimensional RNA-seq data were analyzed with an interactive heat map. The target prediction for compounds was extensively mined using SwissTargetPrediction (threshold > 0.1). The target IDs identified as human targets with accurate UniProtKB/ID were retrieved. The ADME parameters, including oral bioavailability and drug-likeness of the compounds, were analyzed using SwissADME. The corresponding targets identified were

searched in DisGeNet to extract information regarding the genes associated with diabetes using the keyword. A Venn diagram analysis was conducted utilizing Venny 2.1.

2.7. Protein–Protein Interaction (PPI) and Functional Association Network Analysis.

The program STRING 3.0 was utilized to conduct the PPI analysis, following the protein target criteria of NetworkAnalyst for hub and module topology analysis (https://www.networkanalyst.ca). The PPI networks, represented as undirected graphs with proteins as nodes and known interactions as edges, were analyzed to illustrate their connectivity. Additional topological and module analysis was performed to identify the main hub proteins, their connections, and collective activities. A minimal interaction network was selected for further hub and module analysis, where the hub proteins represented key roles in essential signaling pathways. The KEGG database was used to assess the functional importance of the proteins identified.

The "connection first approach" was applied to identify the modules, highlighting the seed proteins' log fold change (log FC) values and calculating the relevance of the modules. An enrichment PPI network analysis of the targets was performed to determine Gene Ontology (GO) and pathways in various biological contexts. The functional annotation enrichment analysis was integrated with biological networks based on multiple lines of evidence from different databases, including GO, KEGG, and BioCarta. Normalization of values was applied using a cumulative hypergeometric distribution to calculate kappa scores for the similarity metric, and similarity score-based clustering was conducted following techniques described in the literature [26, 27]. The scoring functions of the interaction network were based on physical interactions from BioGRID to derive genomic interpretations [28, 29]. The program Cytoscape, an open-source software platform, was used to create the networks [30].

2.8. Molecular Docking Analysis.

The analysis of molecular docking was performed following a previously described method [31]. The molecular graphics and analyses were performed using UCSF Chimera, which was developed by the Resource for Biocomputing, Visualization, and Informatics at the University of California, San Francisco (USA). The docking program AutoDock Vina 1.1.2 was employed to dock four peptides with α-glucosidase and to examine their binding mechanisms. The crystal structures of human pancreatic α-amylase (PDB-1B2Y) and human lysosomal α-glucosidase (PDB-5NN8) were obtained from the Protein Data Bank (PDB: https://www.rcsb.org/) of the Research Collaboratory for Structural Biology (RCSB). Molecular docking studies utilized the positions of the natural ligands, acarbose, which were ascertained using x-ray structures as binding sites. The program Dock Prep was used to prepare protein structures in UCSF Chimera. The ligands underwent energy minimization, and then hydrogens and Gasteiger charges were added. The structures were ultimately stored as .mol2 files. The docking input files

were created using the UCSF Chimera AutoDock Tools 1.5.6 package. The α-amylase search grid dimensions were defined as sizes_x: 19.36, size_y: 21.07, and size_z: 25.8, with centers at 19.2577, center_y: 8.60875, and center_z: 47.6245, respectively. The α-glucosidase search grid dimensions were set to sizes_x: 30.5, size_y: 30.5, and size_z: 30.5, with centers at center_x: 12.9149, center_y: −27.0982, and center_z: 93.9821, respectively. The exhaustiveness was assigned a value of 8 with a maximum energy difference of 3 kcal/mol.

2.9. Statistical Analysis.

The statistical analysis was conducted using GraphPad Prism version 8.0.1 (GraphPad Software, San Diego, CA, USA). One-way ANOVA was applied to compare the statistical differences between groups, while Tukey's post hoc test was implemented to assess significance ($p < 0.05$).

3. Results

3.1. Extraction.

The extraction by maceration over 48 h yielded 16.5% for the ethanolic extract (AIE) and 2.8% for the aqueous extract (AIA).

3.2. α-Glucosidase and α-Amylase Inhibition Activity.

The ethanolic extract (AIE) demonstrated strong inhibitory activity against α-glucosidase ($IC_{50} = 74.15 \pm 1.61$ μg/mL) and α-amylase ($IC_{50} = 13.41 \pm 0.71$ μg/mL) when compared with acarbose ($IC_{50} = 146.01 \pm 1.16$; 57.71 ± 1.46 μg/mL, respectively). In contrast, the aqueous extract (AIA) exhibited insignificant inhibition ($IC_{50} > 200$ μg/mL) of both α-glucosidase and α-amylase.

3.3. GDRI.

The control (without the extract) showed a mean glucose concentration of 0.457 ± 0.004 mmol/mL at 6 h, as presented in Table 1. Overall analysis revealed that the AIA extract inhibited greater glucose movement compared to the AIE. Notably, the AIA extract demonstrated a significant reduction in glucose concentration at both 4 and 6 h when compared to the control. These findings suggest that the AI extract reduces gastrointestinal glucose absorption, thereby lowering blood glucose levels.

3.4. Glucose Uptake/Consumption in 3T3-L1 Pre-Adipocyte and L6 Myotube Cells.

An increase in glucose consumption was observed in 3T3-L1 pre-adipocyte cells following treatment with both AIE and AIA, indicating enhanced glucose consumption (Table 2). The AIE exhibited the highest glucose consumption with an EC_{50} value of < 6.25 μg/mL, while the AIA demonstrated moderate activity with an EC_{50} value of 16.19 μg/mL. Both extracts showed significantly higher glucose consumption than metformin ($EC_{50} = 21.19$ μg/mL).

The effect of AI extracts on glucose uptake was assessed using L6 myotube cells, as shown in Figure 1. Results indicated that AIA and AIE enhanced glucose uptake at 100 μg/mL by approximately 2.5-fold compared to the

TABLE 1: Glucose concentrations in the external solution of *Abutilon indicum* (L.) sweet extracts.

Tested samples	Concentration (mmol/mL)		
	2 h	4 h	6 h
Control	0.571 ± 0.004	0.523 ± 0	0.457 ± 0.004
Abutilon indicum (L.) EtOH extract	$0.638 \pm 0.047^{***}$	$0.439 \pm 0.004^{***}$	$0.365 \pm 0.004^{***}$
Abutilon indicum (L.) H$_2$O extract	0.514 ± 0.044	$0.418 \pm 0.004^{***}$	$0.284 \pm 0.004^{***}$

Note: One way ANOVA followed by Tukey test.
$^{***}p < 0.001$ compared with control.

TABLE 2: The effect of *Abutilon indicum* (L.) sweet extracts in glucose consumption on 3T3-L1 cells.

Tested samples	Percentage of glucose consumption at 100 μg/mL	EC$_{50}$ (μg/mL)
Abutilon indicum (L.) EtOH extract	80.10 ± 3.27	$< 6.25^{***}$
Abutilon indicum (L.) H$_2$O extract	63.35 ± 0.91	16.19
Metformin	89.56 ± 2.02	21.19

Note: One-way ANOVA followed by Tukey test.
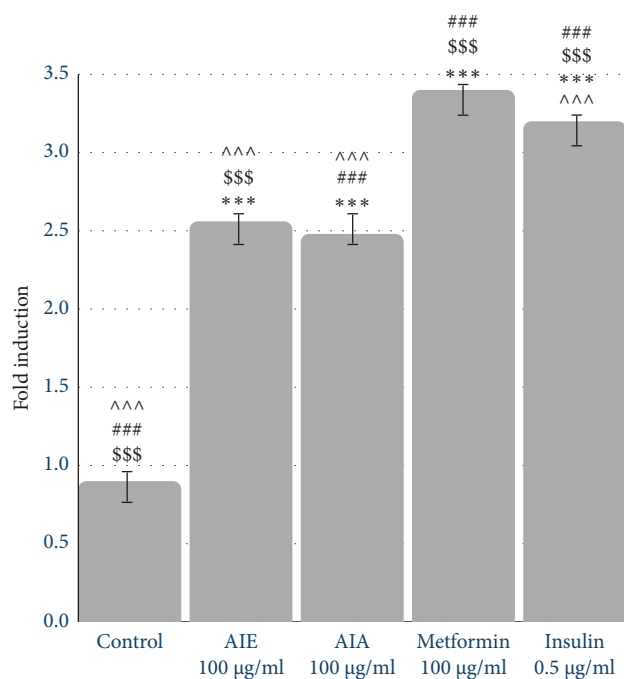$^{***}p < 0.001$ compared with metformin.

FIGURE 1: The effect of *Abutilon indicum* (L.) extracts stimulated glucose uptake in L6 myotube cells one-way ANOVA followed by Tukey test; $^{***}p < 0.001$ compared with control, $^{###}p < 0.001$ compared with AIA, metformin, insulin group comparison with AIE, $^{\$\$\$}p < 0.001$ compares with metformin, insulin group comparisons with AIA, $^{\wedge\wedge\wedge}p < 0.001$ compares insulin group comparison with metformin.

control. AIE exhibited significantly higher glucose uptake than AIA. Patients with type 2 diabetes typically present elevated blood sugar levels due to a decreased insulin-stimulated glucose absorption by cells [16, 17]. These findings suggest that AIE may lower blood sugar levels by stimulating glucose absorption/uptake in both skeletal muscle cells and adipocytes.

3.5. Liquid Chromatography–Mass Spectrometer (LC/QTOF-MS) Analysis.

The AIE was further analyzed using LC-QTOF-MS due to its superior bioactivities compared to the aqueous extract (AIA). This analysis revealed a variety of compounds, which are detailed in Table 3. The LC/QTOF-MS chromatogram is depicted in Figure 2(a) displaying total ion chromatogram and Figure 2(b) showing total compound chromatogram, the identification of 11 distinct compounds. The details of these compounds, including their chemical formula, theoretical mass, observed mass-to-charge ratio (m/z), retention time (RT), mass error (Diff (Tgt, ppm)), score, major MS/MS fragments, and relevant published literature supporting the presence of these compounds, are presented in Table 3. The results confirmed the existence of several phenolic compounds known for their antidiabetic properties, including gallic acid, luteolin, syringic acid, and catechin [38]. Additional bioactive compounds identified included flavonoid glycosides such as rutin, as well as derivatives of coumaric acid like chlorogenic acid, *p*-coumaric acid, and ferulic acid. Other notable compounds included 4-hydroxybenzaldehyde and stigmasterol.

3.6. ADME and Network Pharmacology Analysis.

An investigation into the molecular interactions of AIE with potential protein targets associated with diabetes mellitus was conducted through network pharmacology analysis. This approach aimed to explore the combined effects of the identified compounds and to identify potential mechanistic interactions arising from these combinations [39]. The ADME analysis of LC-MS-identified molecules of AI revealed diverse pharmacokinetic profiles. Absorption: Smaller molecules like gallic acid (MW 170.12), *p*-coumaric acid (MW 164.16), and ferulic acid (MW 194.18) exhibit high GI absorption due to their compliance with Lipinski's rules (0 violations), low molecular weight, and moderate lipophilicity (Consensus Log P 0.21–1.36). In contrast, chlorogenic acid (MW 354.31) and rutin (MW 610.52) show

TABLE 3: List of compounds from ethanolic extract of *Abutilon indicum* (L.) sweet determined by LC-MS/MS-QTOF analysis.

No.	Name	Formula	Theoretical mass	Observed *m/z*	RT	Diff (Tgt, ppm)	Score	Major fragments	Reference
1	Gallic acid	$C_7H_6O_5$	170.0205	170.0216	1.29	0.9	84.21	125.0236, 59.80	[18]
2	Chlorogenic acid	$C_{16}H_{18}O_9$	354.0927	354.0957	1.53	1.9	80.93	255.0, 81.88	[32]
3	*p*-coumaric acid	$C_9H_8O_3$	164.0473	164.0473	18.18	0.6	93.61	147.0438, 63.10	[8]
4	Luteolin	$C_{15}H_{10}O_6$	286.0482	286.0473	18.64	−2.8	87.74	153.0182, 65.44	[33]
5	Syringic acid	$C_9H_{10}O_5$	198.0542	198.0521	19.28	3.2	85	125.0, 74.83	[34]
6	4-Hydroxybenzaldehyde	$C_7H_6O_2$	122.0367	122.0369	21.34	2.21	87.39	123.0442, 21.90	[8]
7	Catechin	$C_{15}H_{14}O_6$	290.077	290.0793	21.65	1.9	89.38	165.0542, 95	[35]
8	Stigmasterol	$C_{29}H_{48}O$	412.3709	413.3772	27.15	0.99	81.65	159.0, 255.0	[8]
9	Ferulic acid	$C_{10}H_{10}O_4$	194.0581	194.0578	27.93	1.1	96.66	177.72, 35	[36]
10	Riboflavin	$C_{17}H_{20}N_4O_6$	376.1383	377.1433	28.60	2.08	52.68	377.1456, 25	[8]
11	Rutin	$C_{27}H_{30}O_{16}$	610.1530	610.1533	28.93	−0.49	85.6	57, 373	[37]
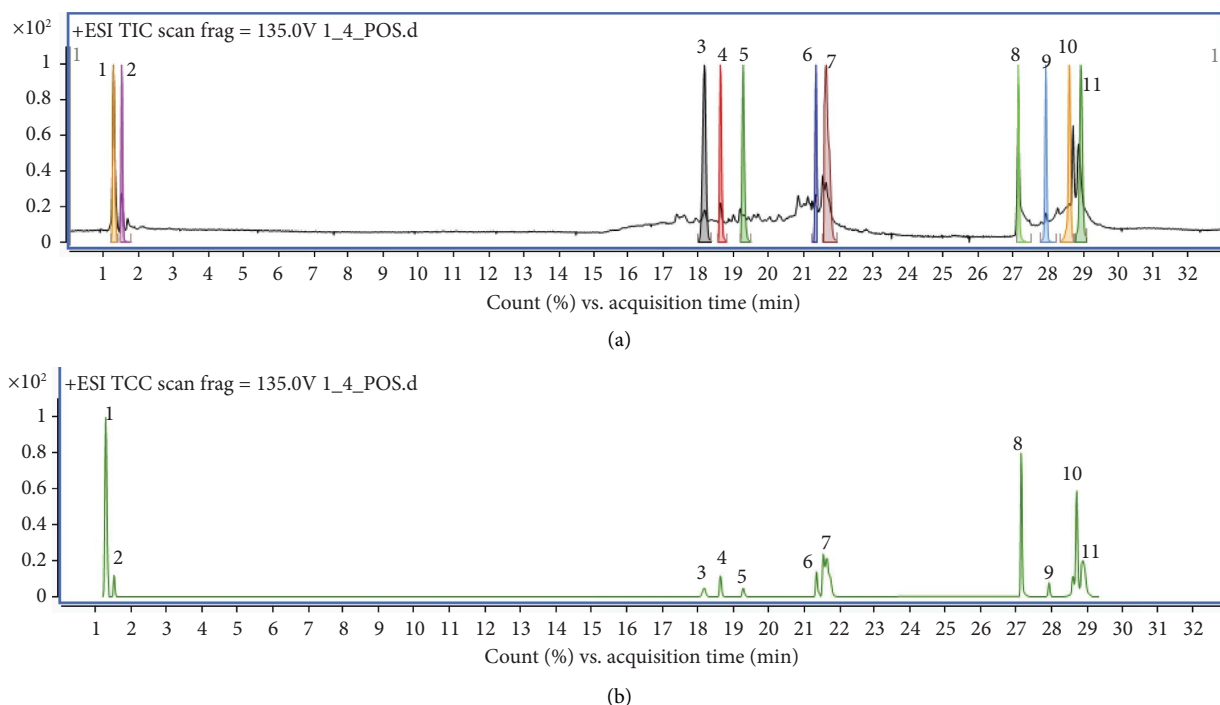
FIGURE 2: LC-QTOF-MS profile of the ethanolic extract of *Abutilon indicum* L. (a) Total ion chromatogram and (b) total compound chromatogram.

low absorption, attributed to their higher molecular weights and multiple Lipinski violations (1 and 3 violations, respectively). Distribution: *p*-Coumaric acid and 4-hydroxybenzaldehyde (TPSA 57.53 and 37.30) demonstrate BBB permeation, likely due to their compact size and lower polar surface area. Larger, polar molecules like rutin (TPSA 269.43) and chlorogenic acid (TPSA 164.75) are restricted from CNS penetration. Metabolism: Luteolin poses a risk as a CYP1A2 and CYP3A4 inhibitor, suggesting potential drug–drug interactions, while others like catechin and stigmasterol show no CYP inhibition. Excretion: Poor solubility (e.g., stigmasterol, ESOL solubility $1.43E − 05$ mg/mL) and high log *P* values (e.g., stigmasterol, Consensus Log *P* 6.98) may hinder renal clearance. Most compounds, however, exhibit favorable solubility (e.g., gallic acid, ESOL class "Very soluble").

Key liabilities include rutin's synthetic complexity (SA 6.52) and stigmasterol's poor solubility. Overall, gallic acid, *p*-coumaric acid, and ferulic acid emerge as promising candidates due to balanced ADME properties.

3.6.1. Target Search and Validation Based on Differential Gene Expression Profiling.

The GEO database was employed to gather and analyze publicly available RNA sequencing data from the muscle tissues of individuals diagnosed with diabetes. This included an analysis of the GSE81965 dataset, which encompassed differentiated myotubes from patients with type 2 diabetes and/or obesity. The dataset provided valuable gene expression data specific to the skeletal muscle [40]. Gene expression data were quantified as gene-level counts using the ARCHS pipeline. The RNA-seq data were categorized into control and treatment groups, facilitating

the identification of differentially expressed targets, which resulted in a total of 16,593 differentially expressed genes. A volcano plot representing the differential expression of these targets is illustrated in Figure 3(a).

The target prediction was accomplished for the 11 compounds identified from the LC-MS-QTOF analysis of A. indicum extract (AIE). A detailed exploration was performed using SwissTargetPrediction, with the threshold set above 0.1. This analysis resulted in the identification of 293 potential targets. Human targets were retrieved with accurate UniProtKB/ID. Furthermore, diabetes-related targets were investigated through DisGeNet, leading to the compilation of a set of 3134 genes based on el-GDA scores greater than 0.9. A Venn diagram presented in Figure 3(b) illustrates the overlap among 103 common targets identified from the GSE81965 dataset, targets from SwissTargetPrediction, NIDDM_GDA-targets derived from gene disease association database for non-insulin dependent diabetes mellitus from DisGeNet disease database, and the compound target search. This diagram emphasizes the substantial intersection between the identified targets and known diabetes-related targets, underscoring the relevance of the compounds in the context of diabetes management.

3.6.2. Target–Compound Network Pathway Enrichment Analysis.

The interacting targets and compounds were utilized to construct the target–compound network depicted in Figure 3(c). The network analysis revealed a complex structure consisting of 307 nodes, comprising 293 targets and 10 compounds interconnected by 356 edges. Key hub targets identified included carbonic anhydrase II (CA2) and glycogen synthase kinase 3 beta (GSK3B), each having 11 connections; pancreatic α-amylase (AMY2A) with 10 connections; insulin-like growth factor 1 receptor (IGF1R) with 8 connections; and PI3-kinase p110-α (PIK3CA) with 7 connections. Notably, luteolin and syringic acid exhibited significant interactions with GSK3B.

Further pathway enrichment analysis was performed using the Fisher exact test (p-value < 0.5) to identify significantly affected biological pathways. This analysis uncovered enriched KEGG pathways associated with the genes interacting with AIE phytochemicals. In addition, Figure 4(a) shows the bubble plot of enriched pathways with hierarchical clustering, and Table 4 presents important pathways related to diabetes among the 103 targets, displayed in a bubble plot alongside hierarchical clustering. The analysis revealed that the compounds in AIE significantly interacted with multiple signaling pathways related to diabetes and associated conditions (Table 4).

The AIE compounds targeted the primary metabolic pathways relevant to diabetes and other conditions associated with impaired glucose or lipid metabolism. These pathways, with a highly significant p-value of 7.78E − 12, are crucial for diabetes management, as disruptions in certain genes may enhance insulin sensitivity [41]. Notable pathways include the PI3K-Akt signaling pathway (p-value = 2.99E − 20), the MAPK signaling pathway (p-value = 6.94E − 15), and pathways related to lipid metabolism and atherosclerosis (p-value = 7.62E − 16).

Moreover, Figure 4(b) illustrates the interaction of AIE compounds with targets within the MAP kinase pathway, including FGFR1, MAPK1, FLT1, IKBKB, MET, MAP3K8, NFKB1, MAPK14, PDGFRB, TEK, IGF1R, AKT1, EGFR, PRKCA, BRAF, INSR, RELA, and IRAK4. Metformin, a potential antidiabetic agent, has been shown to inhibit the MAPK pathway [42]. The regulation of MAPK signaling is crucial in addressing pancreatic β-cell dysfunction and diabetes, as it helps to modulate β-cell function and prevent cell death [43]. Further analysis identified the targets such as PIK3CB, FGFR1, GSK3B, JAK2, MAPK1, FLT1, IKBKB, MET, NFKB1, PDGFRB, TEK, PIK3CA, CDK2, CDK4, IGF1R, AKT1, EGFR, PRKCA, PRKAA2, JAK1, INSR, PIK3CD, RELA, and MTOR that are involved in the PI3K–AKT pathway, as shown in Figure 4(c).

3.6.3. Compound–Target–Protein Interaction Network Enrichment Analysis Reveals the Significance of AIE Targets in Insulin Signaling, Glucose Metabolism, and Transport.

The targets identified that intersect with the disease interaction space, as shown in Figure 5, were examined for crucial PPIs in the STRING interactome. The PPI network initially comprised 580 nodes and 1167 edges, which was further refined to focus on diabetes, resulting in 280 nodes and 645 edges, as illustrated in Figure 5. This refined network was then utilized to elucidate significant functional annotations. The functional enrichments of the targets are represented in pie charts, with colors indicating the most significant functional terms: regulation of metabolic pathways (hsa001100, $p = 5.26E − 21$) is represented in blue; the PI3K–AKT signaling pathway (hsa04151, $p = 9.07E − 11$) is represented in yellow; and insulin resistance (hsa04931, $p = 9.07E − 11$) is represented in pink.

The network analysis of AIE molecules underscores their importance in promoting glucose transport, even in the presence of insulin resistance. The experimental results support this inference, as AIE promotes glucose uptake in L6 myotubes (Figure 1). In addition, Figure 6(a) illustrates the enriched network clustered based on enrichment scores of pathways and GO terms utilized in the analyses. The enriched terms were clustered according to their kappa scores with a similarity greater than 0.3, with nodes representing significant p-values from each of the top clusters connected by edges. Figure 6(b) shows the bar plot of disease enrichment.

The top clusters of the enriched terms are presented in Table 5, where the multi-test-adjusted p-value in logarithmic base 10 is referred to as "Log10(q)" and is computed using standard procedures. Figure 6(b) displays various disease terms enriched among the common targets, including endothelial dysfunction, fatty liver disease, diabetic retinopathy, and more. Finally, Figure 6(c) presents all the GO terms that are crucial for the amelioration of type 2 diabetes.

3.6.4. Molecular Docking Analysis.

The molecular docking study revealed that the top poses of compounds from AIE performed better than acarbose, as demonstrated in Table 6. This table displays the binding affinities, expressed in
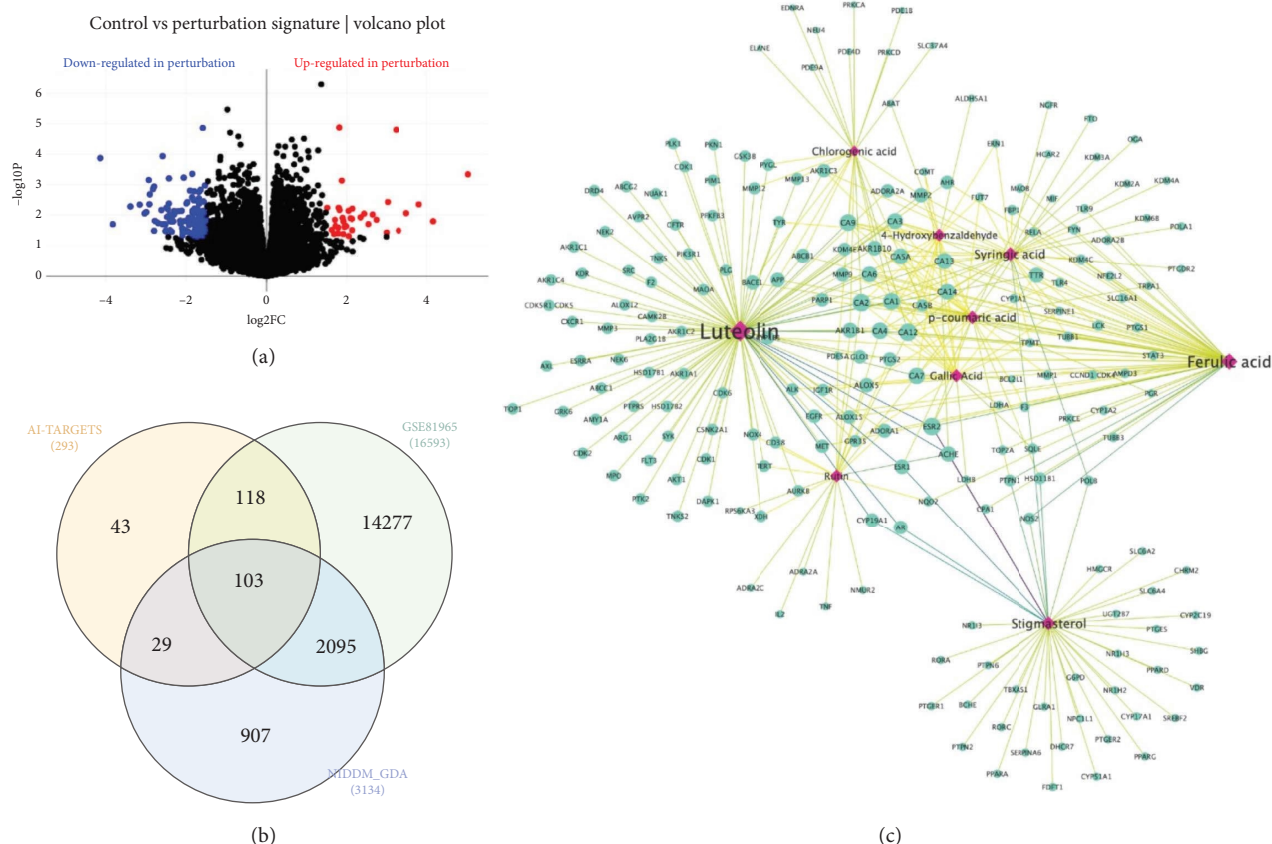
FIGURE 3: (a): Volcano plot of the differential expression of the targets. (b): Venn diagram of target search. AI-*Abuliton indicum* targets from SwissTargetPrediction, NIDDM_GDA-targets derived from gene disease association database for non-insulin-dependent diabetes mellitus from DisGeNet database. (c): Compound–target network with STRING functional association.

kilocalories per mole (kcal/mol), of various ligands for the two human enzymes: pancreatic α-amylase and lysosomal α-glucosidase. Acarbose exhibited a binding affinity of −7.5 kcal/mol for pancreatic α-amylase and −6.4 kcal/mol for lysosomal α-glucosidase. Ligands such as rutin, luteolin, chlorogenic acid, catechin, and stigmasterol demonstrated higher binding affinities for both pancreatic α-amylase and lysosomal α-glucosidase when compared to acarbose. The lower-energy states of these compounds based on the docking poses are illustrated in Figures 7(a), 7(b), 7(c) for human pancreatic α-amylase (PDB ID: 1B2Y) with (a) catechin at −9.1 kcal/mol, (b) stigmasterol at −9.8 kcal/mol, and (c) rutin at −8.9 kcal/mol. In Figures 7(d), 7(e), 7(f), the results for human lysosomal α-glucosidase (PDB ID: 5NN8) are shown with (d) chlorogenic acid at −7.0 kcal/mol, (e) stigmasterol at −8.2 kcal/mol, and (f) rutin at −8.9 kcal/mol.

4. Discussions

The ongoing debate regarding the efficacy and safety of herbal medicines for treating diabetes reflects a pressing need for a deeper understanding of these treatments [44]. While numerous studies indicate positive outcomes, such as enhanced insulin secretion and improved insulin sensitivity from plant-based treatments like A. indicum, significant concerns remain. These concerns center on the variability in

the bioactive compound content, standardization, and potential side effects [10, 19, 45, 46]. Moreover, the interactions between these herbal compounds and conventional antidiabetic drugs are not fully understood, raising questions about their combined use in clinical settings [5, 9, 47].

In the present study, the LC-MS-QTOF and network analysis-based system approaches were employed to molecularly characterize the antidiabetic potential of AIE across various in vitro experiments, including α-glucosidase and α-amylase inhibition, glucose consumption, and glucose uptake in 3T3-L1 adipocytes and L6 skeletal muscle cells. Network analysis elucidated the multi-component mechanisms underlying the antidiabetic effects of AIE, facilitating the identification of targets, ADME profiles, pathways, genes, and disease associations based on PPIs. The enrichment analysis and clustering further clarified the mechanisms of action of the compounds identified by LC-MS-QTOF analysis, correlating them with the in vitro results of α-glucosidase and α-amylase inhibition, glucose consumption, glucose uptake, and cellular viability in 3T3-L1 adipocytes and L6 myotubes.

The observed effects can be attributed to the bioactive flavonoids (rutin, catechin, luteolin) and phenolic compounds (4-hydroxybenzaldehyde, chlorogenic acid, ferulic acid, gallic acid, *p*-coumaric acid, syringic acid) present in AIE, which were identified through the LC-QTOF-MS
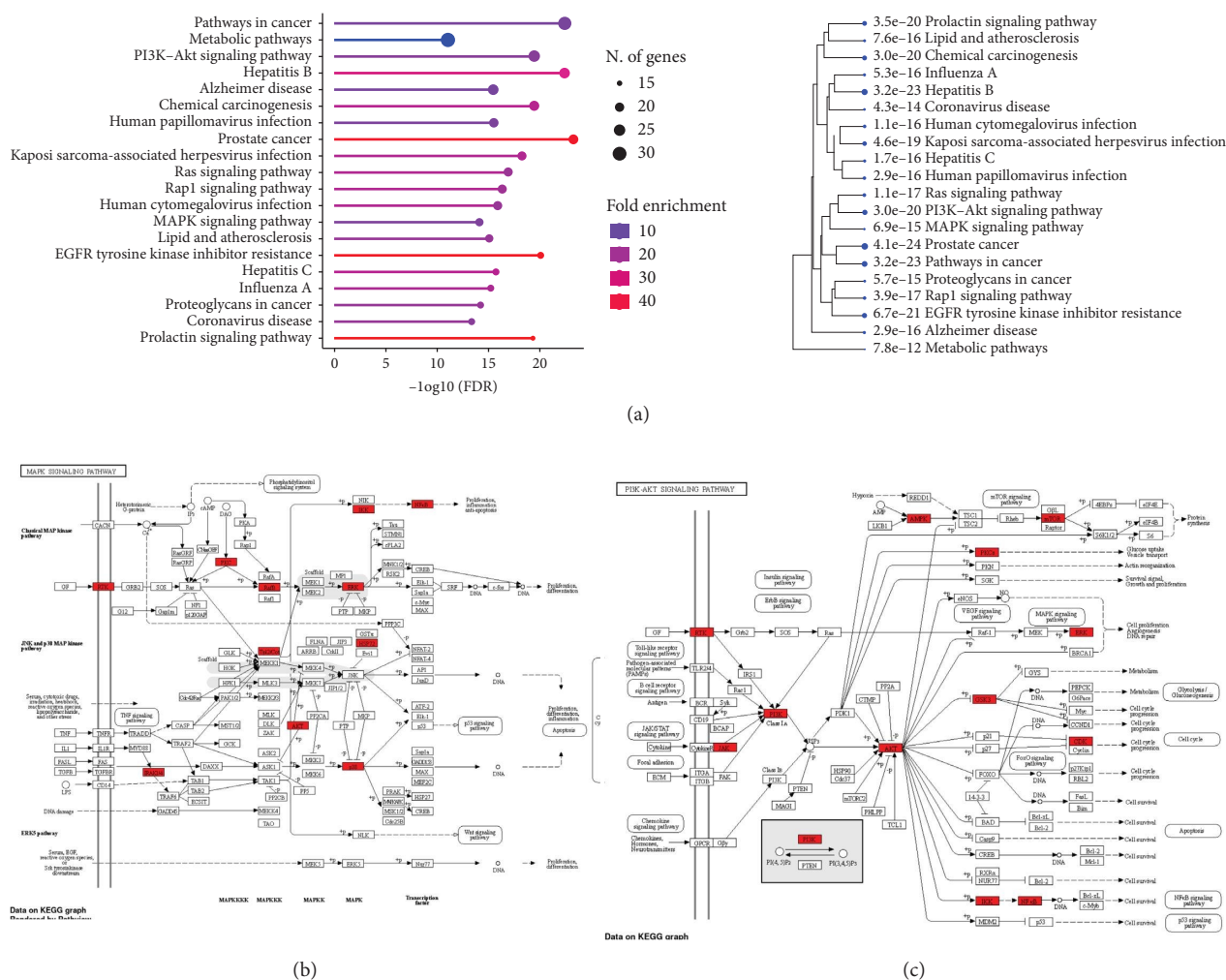
FIGURE 4: (a): Bubble plot of enriched pathways with hierarchical clustering. (b): MAPK signaling pathways. (c): PI3K-AKT signaling pathway.

study, including rutin, luteolin, chlorogenic acid, catechin, and stigmasterol. These compounds are well-documented for their antidiabetic potential, particularly through mechanisms such as free radical scavenging, anti-inflammatory actions, regulation of glucose and lipid metabolism, and management of insulin resistance [48]. The study showed that AIE demonstrated superior activity compared to the aqueous extract, consistent with the identification of 11 compounds that resemble previously reported antidiabetic bioactive compounds, including flavonoids and phenolic compounds [8]. Some specific compounds that were previously identified and isolated from *Abutilon indicum* include *p*-coumaric acid, stigmasterol, and riboflavin [8]. The identified compounds and their reported activities are detailed in Table 7, which emphasizes those compounds that demonstrate significant modulatory effects on glucose metabolism.

The identification of gallic acid in this plant extract was achieved using the HPTLC method [18], while chlorogenic acid was found in another species of *Abutilon* [32]. Luteolin was reported as one of the flavonoid compounds from *A. indicum* flowers [33], and syringic acid was identified in the

methanol extract of the leaves of the plant [34]. Catechins, along with various other flavonoids, were discovered in the seeds of *Abutilon* species [35], and ferulic acid was identified alongside other flavonoids within these species [36]. The flavonoid glycoside rutin, found in the LC-MS-QTOF study, was also previously reported in similar *Abutilon* species [37]. In the experimental results, the AIE demonstrated the ability to inhibit α-glucosidase (IC$_{50}$ = 74.15 ± 1.61 μg/mL) and α-amylase (IC$_{50}$ = 13.41 ± 0.71 μg/mL) more effectively than acarbose, a commonly used antidiabetic drug. These findings align with previous research indicating that the leaves of *A. indicum* possess a robust affinity and potency for inhibiting these enzymes [15]. These results are supported by various studies demonstrating the hypoglycemic and anti-hyperglycemic effects of extracts and isolated compounds from *A. indicum* [61]. The inhibition of these enzymes plays a crucial role in carbohydrate metabolism, as their inhibition can enhance glucose uptake and subsequently promote glycogenesis [62].

Molecular docking studies corroborated the in vitro enzyme inhibition results. These studies revealed that compounds identified in AIE, such as catechin, possess

TABLE 4: Top enriched pathways of AIE phytochemical interacting with targets.

| Pathway	Enrichment FDR	Fold enrichment	Genes
Metabolic pathways	7.78E − 12	4.43	CD38 TYMP PIK3CB PTGS2 PLD1 GSTP1 AKR1B1 GSR ALDH2 HMGCR AKR1A1 HSD11B1 EPHX2 PIK3CA AOC3 CYP19A1 CYP2C9 PDE5A CYP1A1 CYP1A2 CYP17A1 PDE3B XDH ANPEP FASN PIK3CD DHCR7 CA5A PLA2G2A MAOA
PI3K–Akt signaling pathway	2.99E − 20	15.30	PIK3CB FGFR1 GSK3B JAK2 MAPK1 FLT1 IKBKB MET NFKB1 PDGFRB TEK PIK3CA CDK2 CDK4 IGF1R AKT1 EGFR PRKCA PRKAA2 JAK1 INSR PIK3CD RELA MTOR
Ras signaling pathway	1.06E − 17	18.56	PIK3CB PLD1 FGFR1 MAPK1 FLT1 IKBKB MET NFKB1 PDGFRB TEK PIK3CA IGF1R AKT1 EGFR PRKCA INSR PIK3CD RELA PLA2G2A
Rap1 signaling pathway	3.91E − 17	19.34	PIK3CB PRKCZ FGFR1 MAPK1 FLT1 MET MAPK14 PDGFRB TEK PIK3CA IGF1R AKT1 EGFR PRKCA BRAF INSR PIK3CD SRC
MAPK signaling pathway	6.94E − 15	13.81	FGFR1 MAPK1 FLT1 IKBKB MET MAP3K8 NFKB1 MAPK14 PDGFRB TEK IGF1R AKT1 EGFR PRKCA BRAF INSR RELA IRAK4
Lipid and atherosclerosis	7.62E − 16	17.92	PIK3CB GSK3B JAK2 MAPK1 IKBKB NFKB1 MAPK14 PIK3CA CYP2C9 CYP1A1 AKT1 PRKCA PIK3CD RELA MMP1 SRC IRAK4
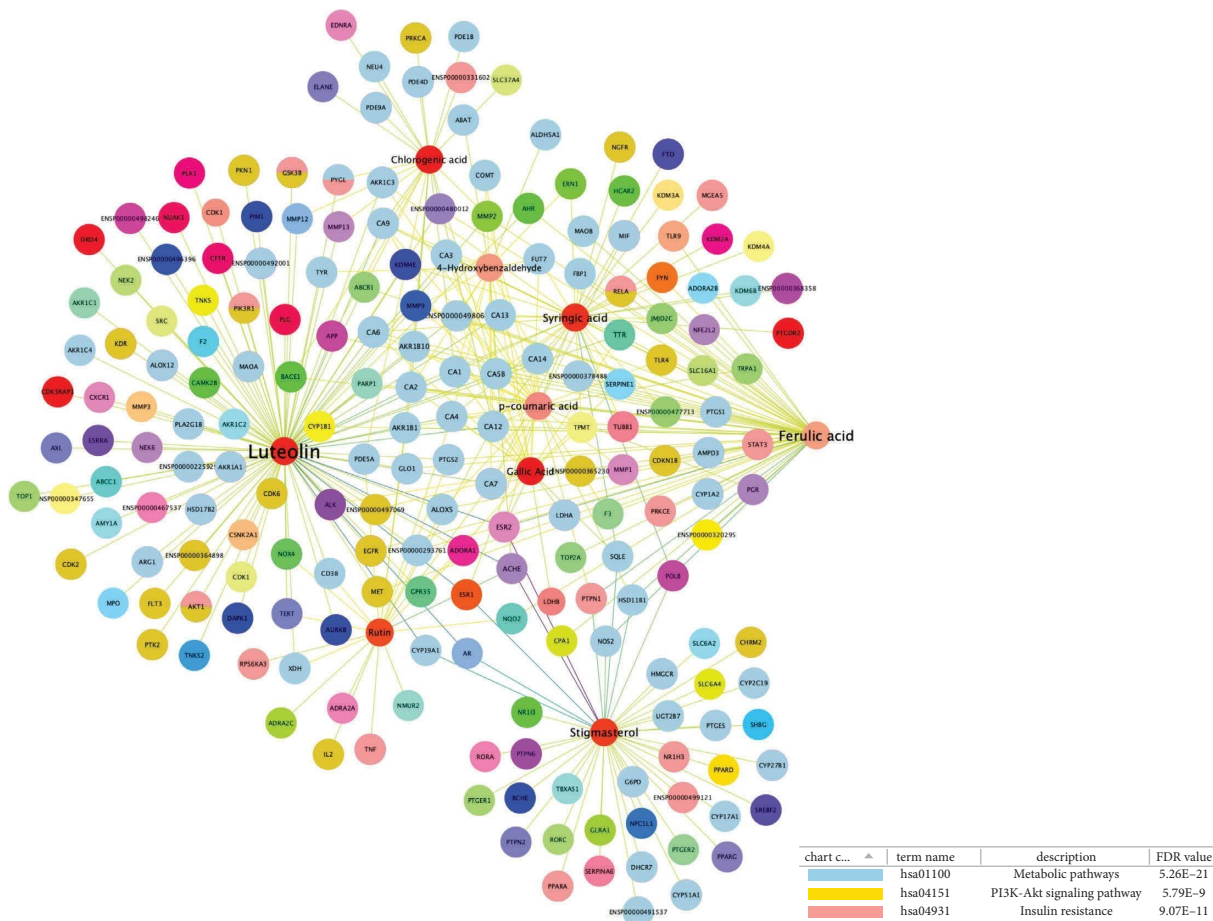
Figure 5: Protein–protein interaction functional enrichment network of AIE.

higher binding affinities for pancreatic α-amylase and lysosomal α-glucosidase compared to acarbose. Catechin demonstrated a binding affinity of −9.1 kcal/mol for pancreatic α-amylase, whereas acarbose showed a binding affinity of −7.5 kcal/mol. This suggests that the antidiabetic potential of AIE may surpass that of acarbose, as these enzymes significantly impact carbohydrate metabolism. The experimental results demonstrated that AIE enhances glucose consumption, with an EC_{50} value of 6.25 μg/mL in 3T3-L1 cells, compared to the EC_{50} value of 21.19 μg/mL for metformin. Additionally, AIE at a concentration of 100 μg/mL significantly enhanced glucose uptake in L6 cells, showing an increase of approximately 2.56- to 2.48-fold. These activities can be attributed to the phenolic compounds found in AIE, such as gallic acid, luteolin, syringic acid, and catechin. These compounds may enhance insulin secretion, improve insulin sensitivity, inhibit glucose absorption, and modulate glucose metabolism [16].

The network pharmacology analysis (Figure 3(c)) highlighted interactions among the carbonic anhydrase family of proteins (CA1, CA2, CA3, CA4, CA5B, CA6, CA7, CA9, CA13, CA14, CA19) with compounds such as gallic acid, luteolin, syringic acid, and catechin.

Research has indicated that carbonic anhydrase serves as a crucial target in antidiabetic therapy, as it reduces hepatic

glucose production and is involved in hepatic gluconeogenesis [63, 64]. The pathway enrichment analysis (Figure 4(a) and Table 4) revealed the significance of compounds in AIE, such as luteolin, chlorogenic acid, syringic acid, and stigmasterol, all connected to metabolic processes. These connections correlate with their involvement in diabetes and glucose transport. Studies suggest that free fatty acids like stigmasterol act as metabolic hubs linking obesity, insulin resistance, and type 2 diabetes (T2DM), which is an independent risk factor for cardiovascular disease and is associated with the development of islet autoimmunity in type 1 diabetes mellitus [65].

The analysis also showed substantial involvement of the PI3K–Akt and MAPK signaling pathways, along with metabolic pathways related to lipids and atherosclerosis. The MAPK signaling pathway, known for its association with inflammatory, oxidative, and apoptotic processes, plays a crucial role in the development of cardiovascular complications in diabetes [66]. Compounds such as luteolin and syringic acid interact with MAPK1, IKBKB, MAP3K8, MAPK14, IGF1R, AKT1, EGFR, PRKCA, and INSR. Additionally, syringic acid modulates glucose uptake and utilization in L6 myotubes and rat muscle tissue [67].

The network enrichment cluster analysis (Figure 6 and Table 5) revealed enrichment for the terms "GO:0006468
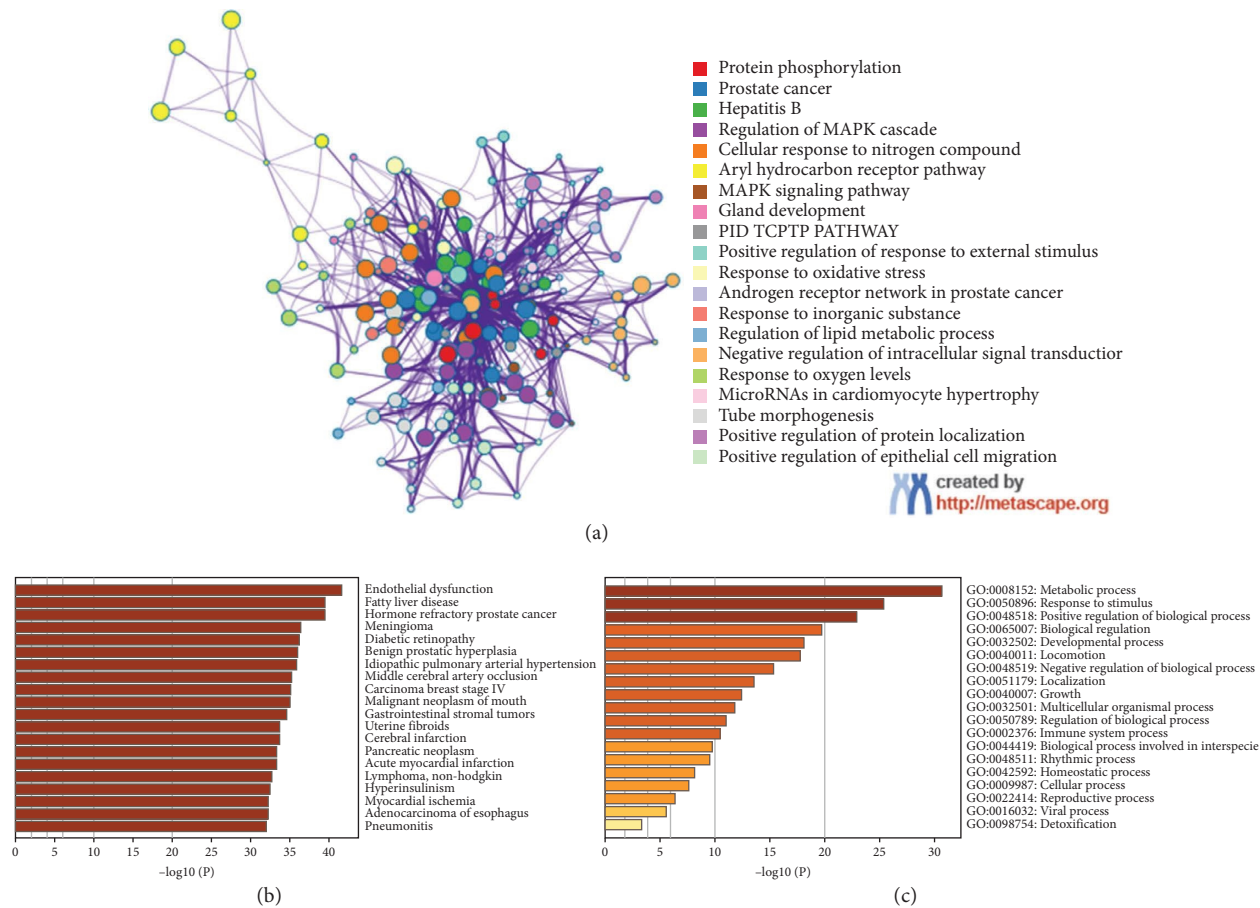
FIGURE 6: (a): Enrichment clustering network. (b): Bar plot of disease enrichment. (c): GO enrichment bar plot.

TABLE 5: Top clusters with their representative-enriched terms involved with AIE target proteins involved in diabetes and associated conditions.

GO	Description	Log10 (P)	Log10 (q)
GO:0006468	Protein phosphorylation	−30.83	−26.49
GO:0043408	Regulation of MAPK cascade	−25.48	−21.91
hsa04010	MAPK signaling pathway	−18.42	−15.81
M91	PID TCPTP PATHWAY	−17.79	−15.27
GO:0032103	Positive regulation of response to external stimulus	−17.08	−14.64
GO:0006979	Response to oxidative stress	−16.44	−14.07
GO:0019216	Regulation of lipid metabolic process	−15.52	−13.2
GO:1902532	Negative regulation of intracellular signal transduction	−15.45	−13.13
GO:0070482	Response to oxygen levels	−15.02	−12.74
WP1544	MicroRNAs in cardiomyocyte hypertrophy	−14.78	−12.52

protein phosphorylation," "GO:0043408 regulation of MAPK cascade," and "hsa04010 MAPK signaling pathway." These terms highlight the importance of promoting the transcription of glucose transporter genes Glut1 and Glut4. The P38 MAPK pathway enhances both insulin-dependent and -independent glucose transport. Additionally, PGC1 is induced by p-38/MAPK, boosting oxidative metabolism by co-activating mitochondrial biogenesis. AMPK and p38 MAPK are co-expressed in the contracting skeletal muscle, where their combined actions promote glucose uptake via insulin-dependent mechanisms [66].

The T cell protein tyrosine phosphatase (TCPTP) pathway, which dephosphorylates substrates like JAK-STAT and insulin receptors (IRs), was found to be significantly enriched. In the liver, TCPTP dephosphorylates STAT3, STAT5, and AKT, regulating insulin signaling by inhibiting key enzymes involved in gluconeogenesis, thus reducing hepatic glucose production [68]. Both network pharmacology and experimental evidence indicate that AIE molecules can inhibit TCPTP, thereby modulating glucose metabolism. Specifically, gallic acid has been shown to restore insulin resistance by enhancing glucose uptake. It

TABLE 6: Molecular docking study of human pancreatic alpha-amylase (1B2Y) and human lysosomal alpha-glucosidase (5NN8) with molecules found in the LC-MS-QTOF study.

Ligands	Human pancreatic alpha-amylase (PDB ID-1B2Y) (kcal/mol)	Human lysosomal alpha glucosidase (PDB ID-5NN8) (kcal/mol)
Acarbose	−7.5	−6.4
Gallic acid	−6.2	−6.0
Chlorogenic acid	−8.0	−7.0
p-coumaric acid	−6.2	−5.7
Luteolin	−8.9	−7.0
Syringic acid	−5.7	−5.5
4-Hydroxybenzaldehyde	−5.0	−5.2
Catechin	−9.1	−6.7
Stigmasterol	−9.8	−8.2
Ferulic acid	−6.4	−5.8
Riboflavin	−8.1	−6.8
Rutin	−8.9	−8.9
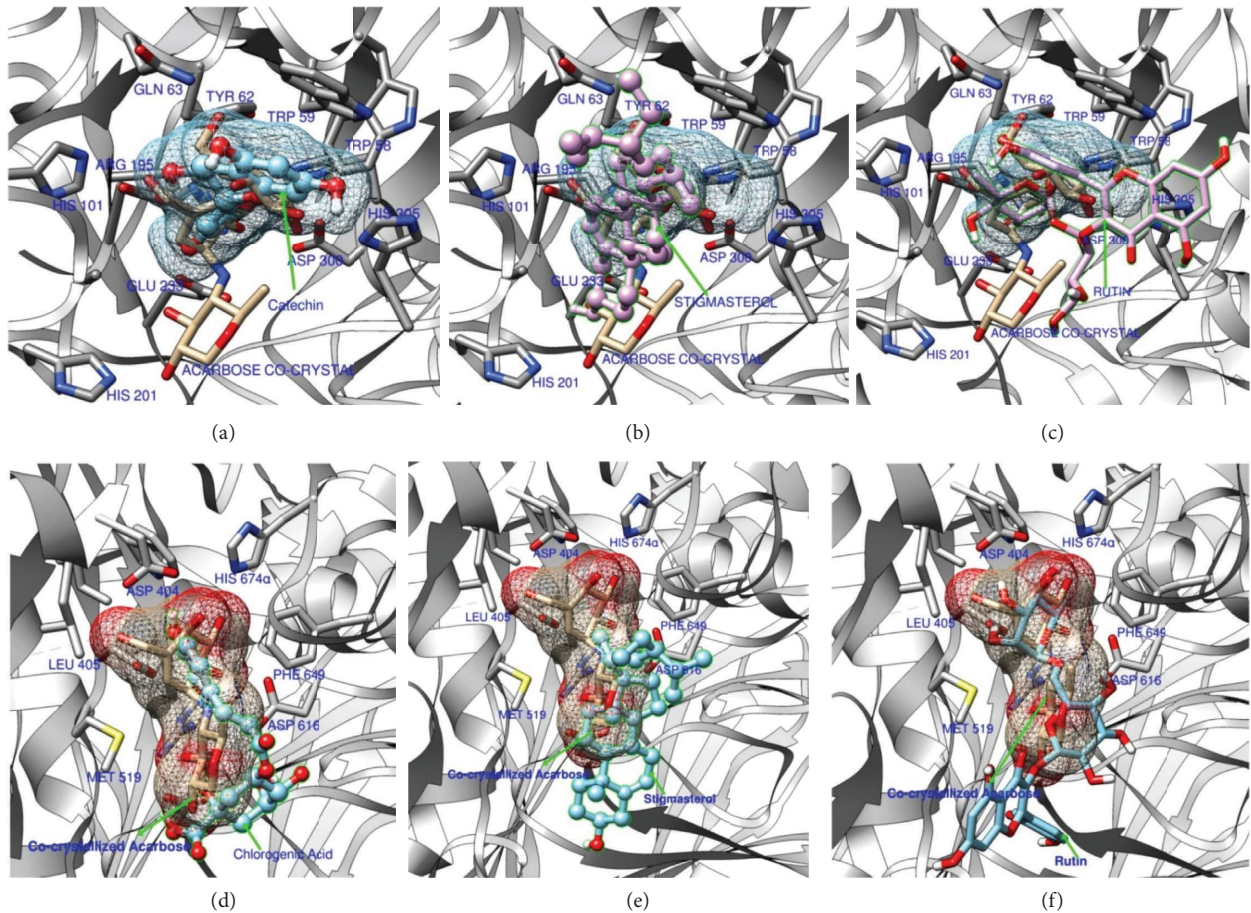
FIGURE 7: Molecular docking study on human pancreatic α-amylase (1B2Y) with (a) catechin, (b) stigmasterol, (c) rutin and human lysosomal α-glucosidase (5NN8) with (d) chlorogenic acid, (e) stigmasterol, and (f) rutin.

reduces oxidative stress that hinders insulin sensitivity by inhibiting the PI3K–Akt signaling pathway, ultimately promoting the translocation of glucose transporter 4 (GLUT4) to the plasma membrane for glucose absorption [69]. The presence of gallic acid in AIE, as confirmed by the LC-MS-QTOF study, supports its role in enhancing insulin

sensitivity and managing glucose metabolism. Gallic acid is known for inhibiting glucose-metabolizing enzymes [61]. Prior studies have quantified gallic acid in the AI methanol extract [18]. The findings from our LC-MS-QTOF analysis also confirmed the presence of gallic acid, which aligns with previous results from animal studies showing its potential

TABLE 7: Reported activity of identified compounds on glucose metabolism.

Compound	Reported activity	Effects on glucose metabolism	References
Gallic acid	Antioxidant, anti-inflammatory, antidiabetic	Enhances insulin secretion, improves glucose uptake, reduces oxidative stress	[49]
Chlorogenic acid	Antioxidant, anti-inflammatory, glucose metabolism modulator	Inhibits glucose absorption, improves insulin sensitivity, reduces postprandial glucose	[50, 51]
p-Coumaric acid	Antioxidant, anti-inflammatory	Improves insulin sensitivity, reduces fasting glucose levels	[52]
Luteolin	Antioxidant, anti-inflammatory, antidiabetic	Enhances insulin sensitivity, modulates glucose transporters	[53]
Syringic acid	Antioxidant, anti-inflammatory	Regulates glucose metabolism, improves pancreatic beta-cell function	[54, 55]
4-Hydroxybenzaldehyde	Antioxidant, anti-inflammatory	Limited direct evidence on glucose metabolism; potential role in reducing inflammation	[56]
Catechin	Antioxidant, anti-inflammatory, cardioprotective	Increases glucose uptake in muscle cells, improves insulin sensitivity	[51]
Stigmasterol	Hypolipidemic, anti-inflammatory	Reduces hyperglycemia, improves insulin sensitivity	[57]
Ferulic acid	Antioxidant, anti-inflammatory, antidiabetic	Enhances insulin secretion, reduces oxidative stress in beta cells	[58]
Riboflavin	Vitamin, antioxidant, coenzyme	Limited direct evidence on glucose metabolism; essential for energy metabolism	[59]
Rutin	Antioxidant, anti-inflammatory, antidiabetic	Improves glucose metabolism, increases GLUT4 translocation in muscle cells	[60]

effects on glucose metabolism [70]. The experimental results revealed the presence of *p*-coumaric acid, which, like gallic acid, has demonstrated antidiabetic effects [71].

Similarly, luteolin has been reported to improve glucose consumption by activating GLUT4 and modulating the PI3K/Akt/GLUT4 signaling pathways in insulin-resistant cells [53]. This aligns with our experimental results, which showed significant enhancement of the PI3K–Akt signaling pathways. Syringic acid and catechin further contribute to the antidiabetic effects of AIE by enhancing glucose transport and inhibiting carbohydrate-metabolizing enzymes, further supporting the in silico and experimental results. Syringic acid is also recognized for its enzyme inhibition potential related to carbohydrate metabolism in various diabetes animal models [55, 72]. Catechin was identified in the LC-MS-QTOF study, which enhanced glucose transport by activating the AMPK and PI3K, thereby improving insulin sensitivity and promoting glucose uptake by cells, as supported by both the in silico and experimental findings [73]. Catechin is also found to interact with human pancreatic α-amylase (PDB ID: 1B2Y) with a docking score of -9.1 kcal/mol compared to -7.5 kcal/mol for acarbose (Figure 7 and Table 6).

Ferulic acid helps in diabetes through various mechanistic pathways [74]. Previous animal studies indicated that at a dosage of 50 mg/kg, the hyperglycemic state in the cardiac tissue of diabetic rats was altered by the increased translocation of GLUT-4 to the cardiac membrane. This alteration was achieved through elevated phosphorylation of PI3K, AKT, and inactivation of GSK-3 [75]. Further studies have also highlighted the anti-hyperglycemic potential of these compounds, which were identified in our LC-MS-QTOF study [76]. Rutin has shown a very stable docking score of -8.9 kcal/mol for both human pancreatic α-amylase (PDB ID: 1B2Y) and human lysosomal α-glucosidase (PDB ID: 5NN8). Moreover, rutin, which demonstrated this stable docking score for these enzymes, has been proven in clinical trials to improve various metabolic parameters in patients with type 2 diabetes mellitus (T2DM) [77]. Rutin, a flavonoid glycoside, has been shown to increase tissue glucose uptake [59]. This suggests that the effects of these bioactive compounds may extend beyond the gastrointestinal tract, potentially offering a more comprehensive antidiabetic strategy through the modulation of multiple pathways involved in diabetes mellitus [62].

The network pharmacology analysis (Figure 5) revealed that luteolin interacts with GSK3A/B, while stigmasterol interacts with PPARG. These interactions represent viable targets for treating diabetes-associated inflammation [78]. The PI3K/AKT signaling pathway is crucial in energy metabolism concerning obesity, insulin resistance, hyperglycemia, and diabetes [79]. The insulin-independent signaling molecule AMPK has been found to reduce high-phosphoinositide-induced activation of the PI3K/AKT/GLUT4 pathway and glucose uptake in myotubes exposed to elevated glucose levels. The activation of the phospho-PI3K/phospho-AKT/phospho-AMPK/GLUT4 signaling cascade is associated with improvements in body weight, fasting blood sugar, glycated hemoglobin, insulin resistance, and glucose intolerance, offering potential treatment strategies

for hyperglycemia. Previous studies reported that activation of the PI3K/AKT/GLUT4 signaling pathway promotes hypoglycemic effects in L6 cells [68] and enhances glucose absorption while reducing insulin resistance in skeletal muscle cells. The glucose-modulating and antioxidant effects of *A. indicum* align with findings from *Rhinacanthus nasutus*, where rhinacanthin-rich extracts enhanced glucose uptake and exhibited antiglycation activity, suggesting shared mechanisms in mitigating metabolic and oxidative stress [80], the multi-target potential of germacrone [81], and the antioxidant properties of *Berberis lycium* [82], underscoring the broader therapeutic promise of phytochemicals in addressing multifactorial diseases like diabetes. Notably, AIE was found to be more effective than metformin in increasing glucose uptake in L6 myotube skeletal muscle cells. This finding suggests that a combination of AIE bioactive natural products (gallic acid, luteolin, syringic acid, and catechin) may be more effective than metformin alone through a multi-combinatorial mechanism of action.

5. Conclusions

The ethanolic extract of *Abutilon indicum* (AIE) exhibits significant antidiabetic potential, attributed to its rich composition of bioactive phenolic compounds, including gallic acid, luteolin, syringic acid, catechin, ferulic acid, and rutin. These compounds work synergistically to enhance glucose metabolism by promoting both glucose consumption and uptake in adipocytes and skeletal muscle cells. This activity is crucial for improving glucose homeostasis pertinent to T2DM. Notably, AIE demonstrated superior inhibitory effects on α-glucosidase and α-amylase enzymes compared to the standard drug acarbose. This indicates its efficacy in modulating carbohydrate digestion and absorption, which were further validated by molecular docking studies. The network pharmacology analyses revealed that phytochemicals present in AIE interact with key protein targets, including PIK3CA, various MAP kinases, GSK3B, carbonic anhydrases (CAs), DPP4, and the insulin receptor (INSR). These interactions predominantly influence the MAP kinase and PI3K–AKT signaling pathways, both of which are critical in regulating glucose metabolism and insulin sensitivity. While these findings provide a robust framework for elucidating the multifaceted antidiabetic mechanisms of AIE, they also pave the way for future research efforts. Subsequent studies that incorporate transcriptomic analyses, protein expression evaluations through Western blotting, and comprehensive in vivo studies in diabetic animal models will be instrumental in validating and expanding upon these preliminary insights. Such research will enhance the understanding of the therapeutic potential of AIE and its role in the management of diabetes.

Nomenclature

2-NBDG	(2-[N-(7-nitrobenz-2-oxa-1,3-diazol-4-yl) amino]-2-deoxy-D-glucose)
3T3-L1	Mouse pre-adipocyte cell line
AIA	Aqueous extract of *Abutilon indicum*

AIE	Ethanolic extract of *Abutilon indicum*
ADME	Absorption, distribution, metabolism, elimination
AMY2A	Pancreatic α-amylase
CA2	Carbonic anhydrase II
GDRI	Glucose diffusion retardation index
GEO	Gene expression omnibus
GSK3B	Glycogen synthase kinase
HPLC-DAD	High-performance liquid chromatography with diode-array detection
IGF1R	Insulin-like growth factor 1 receptor
L6	Rat skeletal muscle cell line
PIK3CA	PI3-kinase p110-α
QTOF-MS	Quadrupole time-of-flight mass spectrometry

Data Availability Statement

All data used to support the findings of this study are included in the article.

Conflicts of Interest

The authors declare no conflicts of interest.

Author Contributions

S.B. contributed to data curation, investigation, methodology, formal analysis, resources, and writing of the original draft. P.P. contributed to data curation, investigation, data analysis, methodology, resources, visualization, and writing – review and editing. W.J. and N.R. contributed to investigation and resources. T.D. contributed to validation and visualization. K.M. contributed to investigation. W.M. and S.L. contributed to formal analysis and visualization. V.S. contributed to formal analysis. S.R., S.H.M., and K.K.C. contributed by reviewing and editing. S.D.S. and L.N. contributed by reviewing and final editing. R.C. contributed to conceptualization, investigation, data curation, funding acquisition, methodology, project administration, writing of the original draft, and final editing.

Declaration of Generative AI and AI-Assisted Technologies in the Writing Process. During the preparation of this work, the author(s) used Grammarly: Free AI Writing Assistance in order to check spelling and grammar. After using this tool/service, the author(s) reviewed and edited the content as needed and take(s) full responsibility for the content of the published article.

References

[1] S. Odeyemi and J. Dewar, "In Vitro Antidiabetic Activity Affecting Glucose Uptake in HepG2 Cells Following Their Exposure to Extracts of Lauridia Tetragona (L.f.) R.H. Archer," *Processes* 8, no. 1 (2019): 33, https://doi.org/10.3390/pr8010033.

[2] M. Mirabelli, E. Chiefari, L. Puccio, D. P. Foti, and A. Brunetti, "Potential Benefits and Harms of Novel Antidiabetic Drugs During COVID-19 Crisis," *International Journal of Environmental Research and Public Health* 17, no. 10 (2020): 3664, https://doi.org/10.3390/ijerph17103664.

[3] C.-T. Wu, P. V. Lidsky, Y. Xiao, et al., "SARS-CoV-2 Infects Human Pancreatic β Cells and Elicits β Cell Impairment," *Cell Metabolism* 33, no. 8 (2021): 1565–1576.e5, https://doi.org/10.1016/j.cmet.2021.05.013.

[4] A. D. Dahlén, G. Dashi, I. Maslov, et al., "Trends in Antidiabetic Drug Discovery: FDA Approved Drugs, New Drugs in Clinical Trials and Global Sales," *Frontiers in Pharmacology* 12 (2022): https://doi.org/10.3389/fphar.2021.807548.

[5] S. Banerjee, P. Debnath, P. N. Rao, T. B. Tripathy, and P. K. Debnath, "Ayurveda in Changing Scenario of Diabetes Management for Developing Safe and Effective Treatment Choices for the Future," *Journal of Complementary and Integrative Medicine* 12, no. 2 (2015): 101–110, https://doi.org/10.1515/jcim-2014-0012.

[6] P. Debnath, T. Tripathy, S. Anon, et al., "Quality of Life Assessment Among Indian Diabetics Engaging an Ayur-Pharmaco-Epidemiological Design," *Exploratory Animal and Medical Research* 11, no. 1 (2021): 89, https://doi.org/10.52635/EAMR/11.1.89-99.

[7] N. Rujanapun, W. Jaidee, T. Duangyod, et al., "Special Thai Oolong Tea: Chemical Profile and In Vitro Antidiabetic Activities," *Frontiers in Pharmacology* 13 (2022): 797032, https://doi.org/10.3389/fphar.2022.797032.

[8] P.-C. Kuo, M.-L. Yang, P.-L. Wu, et al., "Chemical Constituents from Abutilon Indicum," *Journal of Asian Natural Products Research* 10, no. 7 (2008): 689–693, https://doi.org/10.1080/10286020802016545.

[9] P. K. Mukherjee, S. Banerjee, and A. Kar, "Molecular Combination Networks in Medicinal Plants: Understanding Synergy by Network Pharmacology in Indian Traditional Medicine," *Phytochemistry Reviews* 20, no. 4 (2021): 693–703, https://doi.org/10.1007/s11101-020-09730-4.

[10] S. Mukherjee, S. Bera, S. Banerjee, A. Mitra, and P. Mukherjee, "Ayurveda—Translational Approaches towards Validation as Sustainable Healthcare Practices," *Evidence-Based Validation of Herbal Medicine* (2022): 463–485, https://doi.org/10.1016/B978-0-323-85542-6.00016-0.

[11] W. Guo, M. Li, Y. Dong, et al., "Diabetes is a Risk Factor for the Progression and Prognosis of COVID-19," *Diabetes/Metabolism Research and Reviews* 36, no. 7 (2020): e3319, https://doi.org/10.1002/dmrr.3319.

[12] F. Huang, J. Mu, Z. Liu, Q. Lin, Y. Fang, and Y. Liang, "The Nutritional Intervention of Ingredients From Food Medicine

Homology Regulating Macrophage Polarization on Athero-sclerosis," *Journal of Agricultural and Food Chemistry* 71 (2023): 20441–20452, https://doi.org/10.1021/acs.jafc.3c06375.

[13] B. Sharma and D. K. Yadav, "Metabolomics and Network Pharmacology in the Exploration of the Multi-Targeted Therapeutic Approach of Traditional Medicinal Plants," *Plants* 11 (2022): 3243, https://doi.org/10.3390/plants11233243.

[14] S. Adisakwattana, K. Pudhom, and S. Yibchok-Anun, "Influence of the Methanolic Extract From *Abutilon indicum* Leaves in Normal and Streptozotocin-Induced Diabetic Rats," *African Journal of Biotechnology* 8 (2009).

[15] F. Arce, J. E. Concepcion, K. Mayol, and G. L. See, in *Vitro α-Amylase and α-Glucosidase Inhibition Activity of Tabing Abutilon Indicum (Linn 1836) Root Extracts* (2016).

[16] C. Krisanapun, P. Peungvicha, R. Temsiririrkkul, and Y. Wongkrajang, "Aqueous Extract of Abutilon Indicum Sweet Inhibits Glucose Absorption and Stimulates Insulin Secretion in Rodents," *Nutrition Research* 29, no. 8 (2009): 579–587, https://doi.org/10.1016/j.nutres.2009.07.006.

[17] C. Krisanapun, S.-H. Lee, P. Peungvicha, R. Temsiririrkkul, and S. J. Baek, "Antidiabetic Activities of *Abutilon indicum* (L.) Sweet Are Mediated by Enhancement of Adipocyte Differentiation and Activation of the GLUT1 Promoter," *Evidence-based Complementary and Alternative Medicine: eCAM* 2011, no. 1 (2011): 167684, https://doi.org/10.1093/ecam/neq004.

[18] M. S. Hussain, S. Fareed, M. Ali, and M. A. Rahman, "Validation of the Method for the Simultaneous Estimation of Bioactive Marker Gallic Acid and Quercetin in Abutilon Indicum by HPTLC," *Asian Pacific Journal of Tropical Disease* 2 (2012): S76–S83, https://doi.org/10.1016/S2222-1808(12)60127-3.

[19] D. Ramadas, S. K. Nune, D. Chikkanna, K. V. Maheshwara, and V. Joshi, "Anti-glycation and Antioxidant Properties of Abutilon Indicum Plant Leaves," *Int. J. Sci. Res. Arch.* 2 (2021): 001–005.

[20] P. Teerapongpisan, V. Suthiphasilp, T. Maneerat, et al., "α-Glucosidase Inhibitory and α-amylase Inhibitory Activities of Compounds Isolated from Uvaria Rufa Blume," *Natural Product Research* 36, no. 23 (2022): 6039–6043, https://doi.org/10.1080/14786419.2022.2041010.

[21] X. Wu and S. Dhanasekaran, "Protective Effect of Leaf Extract of *Abutilon indicum* on DNA Damage and Peripheral Blood Lymphocytes in Combating the Oxidative Stress," *Saudi Pharmaceutical Journal* 28 (2020): 943–950, https://doi.org/10.1016/j.jsps.2020.06.015.

[22] S. Yasmin, M. A. Kashmiri, I. Ahmad, A. Adnan, and M. Ahmad, "Biological Activity of Extracts in Relationship to Structure of Pure Isolates of *Abutilon indicum*," *Pharmaceutical Biology* 46 (2008): 673–676, https://doi.org/10.1080/13880200802215784.

[23] S. Yasmin, M. A. Kashmiri, M. N. Asghar, M. Ahmad, and A. Mohy-ud-Din, "Antioxidant Potential and Radical Scavenging Effects of Various Extracts From *Abutilon indicum* and *Abutilon muticum*," *Pharmaceutical Biology* 48 (2010): 282–289, https://doi.org/10.3109/13880200903110769.

[24] S. Thengyai, P. Thiantongin, C. Sontimuang, C. Ovatlarnporn, and P. Puttarak, "α-Glucosidase and α-amylase Inhibitory Activities of Medicinal Plants in Thai Antidiabetic Recipes and Bioactive Compounds from *Vitex glabrata* R," *Journal of Herbal Medicine* 19 (2020): 100302, https://doi.org/10.1016/j.hermed.2019.100302.

[25] C. M. N. Picot, A. H. Subratty, and M. F. Mahomoodally, "Inhibitory Potential of Five Traditionally Used Native Antidiabetic Medicinal Plants on α-Amylase, α-Glucosidase, Glucose Entrapment, and Amylolysis Kinetics In Vitro," *Advances in Pharmacological Sciences* 2014 (2014): 739834, https://doi.org/10.1155/2014/739834.

[26] J. Cohen, "A Coefficient of Agreement for Nominal Scales," *Educational and Psychological Measurement* 20, no. 1 (1960): 37–46, https://doi.org/10.1177/001316446002000104.

[27] Y. Hochberg and Y. Benjamini, "More Powerful Procedures for Multiple Significance Testing," *Statistics in Medicine* 9, no. 7 (1990): 811–818, https://doi.org/10.1002/sim.4780090710.

[28] T. Li, R. Wernersson, R. B. Hansen, et al., "A Scored Human Protein-Protein Interaction Network to Catalyze Genomic Interpretation," *Nature Methods* 14, no. 1 (2017): 61–64, https://doi.org/10.1038/nmeth.4083.

[29] C. Stark, B.-J. Breitkreutz, T. Reguly, L. Boucher, A. Breitkreutz, and M. Tyers, "BioGRID: a General Repository for Interaction Datasets," *Nucleic Acids Research* 34, no. Database issue (2006): D535–D539, https://doi.org/10.1093/nar/gkj109.

[30] P. Shannon, A. Markiel, O. Ozier, et al., "Cytoscape: a Software Environment for Integrated Models of Biomolecular Interaction Networks," *Genome Research* 13, no. 11 (2003): 2498–2504, https://doi.org/10.1101/gr.1239303.

[31] Q. Zhao, G. Wei, K. Li, S. Duan, R. Ye, and A. Huang, "Identification and Molecular Docking of Novel α-Glucosidase Inhibitory Peptides From Hydrolysates of Binglangjiang Buffalo Casein," *Lebensmittel-Wissenschaft & Technologie* 156 (2022): 113062, https://doi.org/10.1016/j.lwt.2021.113062.

[32] S. Shi, J. Cheng, N. Ahmad, et al., "Effects of Potential Allelochemicals in a Water Extract of Abutilon Theophrasti Medik. On Germination and Growth of Glycine Max L., Triticum aestivum L., and Zea mays L," *Journal of the Science of Food and Agriculture* 103, no. 4 (2023): 2155–2165, https://doi.org/10.1002/jsfa.12315.

[33] I. Matławska and M. Sikorska, "Flavonoid Compounds in the Flowers of Abutilon Indicum (L.) Sweet (Malvaceae)," *Acta Poloniae Pharmaceutica* 59, no. 3 (2002): 227–229.

[34] R. S. Khan, M. Senthi, P. C. Rao, et al., "Cytotoxic Constituents of Abutilon Indicum Leaves against U87MG Human Glioblastoma Cells," *Natural Product Research* 29, no. 11 (2015): 1069–1073, https://doi.org/10.1080/14786419.2014.976643.

[35] W. L. Paszkowski and R. J. Kremer, "Biological Activity and Tentative Identification of Flavonoid Components in Velvetleaf (Abutilon Theophrasti Medik.) Seed Coats," *Journal of Chemical Ecology* 14, no. 7 (1988): 1573–1582, https://doi.org/10.1007/BF01012523.

[36] B. Ali, M. Imran, R. Hussain, Z. Ahmed, and A. Malik, "Structural Determination of Abutilins A and B, New Flavonoids from Abutilon Pakistanicum, by 1D and 2D NMR Spectroscopy," *Magnetic Resonance in Chemistry* 48, no. 2 (2010): 159–163, https://doi.org/10.1002/mrc.2546.

[37] C. Tian, P. Zhang, C. Yang, et al., "Extraction Process, Component Analysis, and In Vitro Antioxidant, Antibacterial, and Anti-inflammatory Activities of Total Flavonoid Extracts from Abutilon Theophrasti Medic. Leaves," *Mediators of Inflammation* 2018 (2018): 1–17, https://doi.org/10.1155/2018/3508506.

[38] V. B. Tatipamula and B. Kukavica, "Phenolic Compounds as Antidiabetic, Anti-inflammatory, and Anticancer Agents and

Improvement of Their Bioavailability by Liposomes," *Cell Biochemistry and Function* 39, no. 8 (2021): 926–944, https://doi.org/10.1002/cbf.3667.

[39] S. Kulshrestha, A. Goel, S. Banerjee, R. Sharma, M. R. Khan, and K.-T. Chen, "Metabolomics and Network Pharmacology–Guided Analysis of TNF-α Expression by Argemone Mexicana (Linn) Targeting NF-kB the Signalling Pathway in Cancer Cell Lines," *Frontiers in Oncology* 14 (2024): 1502819, https://doi.org/10.3389/fonc.2024.1502819.

[40] L. Väremo, T. I. Henriksen, C. Scheele, et al., "Type 2 Diabetes and Obesity Induce Similar Transcriptional Reprogramming in Human Myocytes," *Genome Medicine* 9, no. 1 (2017): 47, https://doi.org/10.1186/s13073-017-0432-2.

[41] E. S. Goetzman, Z. Gong, M. Schiff, Y. Wang, and R. H. Muzumdar, "Metabolic Pathways at the Crossroads of Diabetes and Inborn Errors," *Journal of Inherited Metabolic Disease* 41, no. 1 (2018): 5–17, https://doi.org/10.1007/s10545-017-0091-x.

[42] X. He, F. Gao, J. Hou, et al., "Metformin Inhibits MAPK Signaling and Rescues Pancreatic Aquaporin 7 Expression to Induce Insulin Secretion in Type 2 Diabetes Mellitus," *Journal of Biological Chemistry* 297 (2021): 101002, https://doi.org/10.1016/j.jbc.2021.101002.

[43] V. Sidarala and A. Kowluru, "The Regulatory Roles of Mitogen-Activated Protein Kinase (MAPK) Pathways in Health and Diabetes: Lessons Learned from the Pancreatic β-Cell," *Recent Patents on Endocrine, Metabolic & Immune Drug Discovery* 10, no. 2 (2017): 76–84, https://doi.org/10.2174/1872214810666161020154905.

[44] A. Balkrishna, N. Sharma, D. Srivastava, A. Kukreti, S. Srivastava, and V. Arya, "Exploring the Safety, Efficacy, and Bioactivity of Herbal Medicines: Bridging Traditional Wisdom and Modern Science in Healthcare," *Future Integrative Medicine* 3, no. 1 (2024): 35–49, https://doi.org/10.14218/FIM.2023.00086.

[45] A. Kar, P. K. Mukherjee, S. Saha, et al., "Metabolite Profiling and Evaluation of CYP450 Interaction Potential of 'Trimada'-An Ayurvedic Formulation," *Journal of Ethnopharmacology* 266 (2021): 113457, https://doi.org/10.1016/j.jep.2020.113457.

[46] H. Zwickey, A. Horgan, D. Hanes, et al., "Effect of the Anti-Inflammatory Diet in People with Diabetes and Pre-Diabetes: A Randomized Controlled Feeding Study," *Journal of Restorative Medicine* 8, no. 1 (2019): e20190107, https://doi.org/10.14200/jrm.2019.0107.

[47] T. Rao, J. Peng, Y. Guo, Y. Chen, H. Zhou, and D. Ouyang, "The Pharmacogenetics of Natural Products: A Pharmacokinetic and Pharmacodynamic Perspective," *Pharmacological Research* 146 (2019): 104283, https://doi.org/10.1016/j.phrs.2019.104283.

[48] X. Yi, M. Dong, N. Guo, et al., "Flavonoids Improve Type 2 Diabetes Mellitus and its Complications: a Review," *Frontiers in Nutrition* 10 (2023): 1192131, https://doi.org/10.3389/fnut.2023.1192131.

[49] Y. Xu, G. Tang, C. Zhang, N. Wang, and Y. Feng, "Gallic Acid and Diabetes Mellitus: Its Association with Oxidative Stress," *Molecules (Basel)* 26, no. 23 (2021): 7115, https://doi.org/10.3390/molecules26237115.

[50] V. Nguyen, E. G. Taine, D. Meng, T. Cui, and W. Tan, "Chlorogenic Acid: A Systematic Review on the Biological Functions, Mechanistic Actions, and Therapeutic Potentials," *Nutrients* 16, no. 7 (2024): 924, https://doi.org/10.3390/nu16070924.

[51] A. Yanagimoto, Y. Matsui, T. Yamaguchi, M. Hibi, S. Kobayashi, and N. Osaki, "Effects of Ingesting Both Catechins and Chlorogenic Acids on Glucose, Incretin, and Insulin Sensitivity in Healthy Men: A Randomized, Double-Blinded, Placebo-Controlled Crossover Trial," *Nutrients* 14, no. 23 (2022): 5063, https://doi.org/10.3390/nu14235063.

[52] D. S. Yoon, S. Y. Cho, H. J. Yoon, S. R. Kim, and U. J. Jung, "Protective Effects of P-Coumaric Acid against High-Fat Diet-Induced Metabolic Dysregulation in Mice," *Biomedicine & Pharmacotherapy* 142 (2021): 111969, https://doi.org/10.1016/j.biopha.2021.111969.

[53] L. Miao, H. Zhang, M. S. Cheong, et al., "Anti-diabetic Potential of Apigenin, Luteolin, and Baicalein via Partially Activating PI3K/Akt/Glut-4 Signaling Pathways in Insulin-Resistant HepG2 Cells," *Food Science and Human Wellness* 12, no. 6 (2023): 1991–2000, https://doi.org/10.1016/j.fshw.2023.03.021.

[54] O. T. Somade, B. E. Oyinloye, B. O. Ajiboye, and O. A. Osukoya, "Syringic Acid Demonstrates an Anti-inflammatory Effect via Modulation of the NF-κB-iNOS-COX-2 and JAK-STAT Signaling Pathways in Methyl Cellosolve-Induced Hepato-Testicular Inflammation in Rats," *Biochemistry and Biophysics Reports* 34 (2023): 101484, https://doi.org/10.1016/j.bbrep.2023.101484.

[55] S. Srinivasan, J. Muthukumaran, U. Muruganathan, R. S. Venkatesan, and A. M. Jalaludeen, "Antihyperglycemic Effect of Syringic Acid on Attenuating the Key Enzymes of Carbohydrate Metabolism in Experimental Diabetic Rats," *Biomedicine & Preventive Nutrition* 4 (2014): 595–602, https://doi.org/10.1016/j.bionut.2014.07.010.

[56] J. O. Unuofin and S. L. Lebelo, "Antioxidant Effects and Mechanisms of Medicinal Plants and Their Bioactive Compounds for the Prevention and Treatment of Type 2 Diabetes: An Updated Review," *Oxidative Medicine and Cellular Longevity* 2020 (2020): 1–36, https://doi.org/10.1155/2020/1356893.

[57] M. G. Ward, G. Li, V. C. Barbosa-Lorenzi, and M. Hao, "Stigmasterol Prevents Glucolipotoxicity Induced Defects in Glucose-Stimulated Insulin Secretion," *Scientific Reports* 7, no. 1 (2017): 9536, https://doi.org/10.1038/s41598-017-10209-0.

[58] K. Ruamyod, W. B. Watanapa, C. Kakhai, P. Nambundit, S. Treewaree, and P. Wongsanupa, "Ferulic Acid Enhances Insulin Secretion by Potentiating L-type Ca2+ Channel Activation," *Journal of Integrative Medicine* 21, no. 1 (2023): 99–105, https://doi.org/10.1016/j.joim.2022.11.003.

[59] N. Suwannasom, I. Kao, A. Pruß, R. Georgieva, and H. Bäumler, "Riboflavin: The Health Benefits of a Forgotten Natural Vitamin," *International Journal of Molecular Sciences* 21, no. 3 (2020): 950, https://doi.org/10.3390/ijms21030950.

[60] A. Gupta, A. Jamal, D. A. Jamil, and H. A. Al-Aubaidy, "A Systematic Review Exploring the Mechanisms by Which Citrus Bioflavonoid Supplementation Benefits Blood Glucose Levels and Metabolic Complications in Type 2 Diabetes Mellitus," *Diabetes & Metabolic Syndrome: Clinical Research Reviews* 17, no. 11 (2023): 102884, https://doi.org/10.1016/j.dsx.2023.102884.

[61] G. Oboh, O. B. Ogunsuyi, M. D. Ogunbadejo, and S. A. Adefegha, "Influence of Gallic Acid on α-amylase and α-glucosidase Inhibitory Properties of Acarbose," *Journal of Food and Drug Analysis* 24, no. 3 (2016): 627–634, https://doi.org/10.1016/j.jfda.2016.03.003.

[62] P. Khanal and B. M. Patil, "Gene Ontology Enrichment Analysis of α-amylase Inhibitors from Duranta Repens in Diabetes Mellitus," *Journal of Diabetes and Metabolic*

Disorders 19, no. 2 (2020): 735–747, https://doi.org/10.1007/s40200-020-00554-9.

[63] I. S. Ismail, "The Role of Carbonic Anhydrase in Hepatic Glucose Production," *Current Diabetes Reviews* 14, no. 2 (2018): 108–112, https://doi.org/10.2174/1573399812666161214122351.

[64] I. S. Ismail, "Metformin-carbonic Anhydrase Interaction Facilitate Lactate Accumulation in Type 2 Diabetes," *Diabetes Management* 7 (2017): 337–342.

[65] J. Zhang, Y. Xiao, J. Hu, S. Liu, Z. Zhou, and L. Xie, "Lipid Metabolism in Type 1 Diabetes Mellitus: Pathogenetic and Therapeutic Implications," *Frontiers in Immunology* 13 (2022): 999108, https://doi.org/10.3389/fimmu.2022.999108.

[66] F. F. Jubaidi, S. Zainalabidin, I. S. Taib, et al., "The Role of PKC-MAPK Signalling Pathways in the Development of Hyperglycemia-Induced Cardiovascular Complications," *International Journal of Molecular Sciences* 23, no. 15 (2022): 8582, https://doi.org/10.3390/ijms23158582.

[67] L. M. Ramorobi, G. R. Matowane, S. S. Mashele, et al., "Zinc(II) – Syringic Acid Complexation Synergistically Exerts Antioxidant Action and Modulates Glucose Uptake and Utilization in L-6 Myotubes and Rat Muscle Tissue," *Biomedicine & Pharmacotherapy* 154 (2022): 113600, https://doi.org/10.1016/j.biopha.2022.113600.

[68] P. Wang, T. He, R. Zheng, et al., "Applying Cooperative Module Pair Analysis to Uncover Compatibility Mechanism of Fangjis: An Example of Wenxin Keli Decoction," *Journal of Ethnopharmacology* 278 (2021): 114214, https://doi.org/10.1016/j.jep.2021.114214.

[69] Q. Xu, Q. Guo, C.-X. Wang, et al., "Network Differentiation: A Computational Method of Pathogenesis Diagnosis in Traditional Chinese Medicine Based on Systems Science," *Artificial Intelligence in Medicine* 118 (2021): 102134, https://doi.org/10.1016/j.artmed.2021.102134.

[70] G. R. Gandhi, G. Jothi, P. J. Antony, et al., "Gallic Acid Attenuates High-Fat Diet Fed-Streptozotocin-Induced Insulin Resistance via Partial Agonism of PPARγ in Experimental Type 2 Diabetic Rats and Enhances Glucose Uptake through Translocation and Activation of GLUT4 in PI3K/p-Akt Signaling Pathway," *European Journal of Pharmacology* 745 (2014): 201–216, https://doi.org/10.1016/j.ejphar.2014.10.044.

[71] A. Abdel-Moneim, A. I. Yousef, S. M. Abd El-Twab, E. S. Abdel Reheim, and M. B. Ashour, "Gallic Acid and P-Coumaric Acid Attenuate Type 2 Diabetes-Induced Neurodegeneration in Rats," *Metabolic Brain Disease* 32, no. 4 (2017): 1279–1286, https://doi.org/10.1007/s11011-017-0039-8.

[72] S. Shimsa, N. P. P. Soumya, S. Mondal, and S. Mini, "Syringic Acid Affords Antioxidant Protection in the Pancreas of Type 2 Diabetic Rats," *Bioactive Compounds in Health and Disease* 6 (2023): 13, https://doi.org/10.31989/bchd.v6i2.1061.

[73] L. Wen, D. Wu, X. Tan, et al., "The Role of Catechins in Regulating Diabetes: An Update Review," *Nutrients* 14, no. 21 (2022): 4681, https://doi.org/10.3390/nu14214681.

[74] X. Li, J. Wu, F. Xu, et al., "Use of Ferulic Acid in the Management of Diabetes Mellitus and its Complications," *Molecules (Basel)* 27, no. 18 (2022): 6010, https://doi.org/10.3390/molecules27186010.

[75] S. Chowdhury, S. Ghosh, K. Rashid, and P. C. Sil, "Deciphering the Role of Ferulic Acid against Streptozotocin-Induced Cellular Stress in the Cardiac Tissue of Diabetic Rats," *Food and Chemical Toxicology* 97 (2016): 187–198, https://doi.org/10.1016/j.fct.2016.09.011.

[76] R. Ramu, P. S. Shirahatti, S. Nayakavadi, et al., "The Effect of a Plant Extract Enriched in Stigmasterol and β-sitosterol on Glycaemic Status and Glucose Metabolism in Alloxan-Induced Diabetic Rats," *Food & Function* 7, no. 9 (2016): 3999–4011, https://doi.org/10.1039/C6FO00343E.

[77] H. Bazyar, L. Moradi, F. Zaman, and A. Zare Javid, "The Effects of Rutin Flavonoid Supplement on Glycemic Status, Lipid Profile, Atherogenic Index of Plasma, Brain-Derived Neurotrophic Factor (BDNF), Some Serum Inflammatory, and Oxidative Stress Factors in Patients with Type 2 Diabetes Mellitus: A Double-Blind, Placebo-Controlled Trial," *Phytotherapy Research* 37, no. 1 (2023): 271–284, https://doi.org/10.1002/ptr.7611.

[78] C. L. Pitasi, J. Liu, B. Gausserès, et al., "Implication of Glycogen Synthase Kinase 3 in Diabetes-Associated Islet Inflammation," *Journal of Endocrinology* 244, no. 1 (2020): 133–148, https://doi.org/10.1530/JOE-19-0239.

[79] X. Jia and W. Liu, "Vaccarin Improves Insulin Sensitivity and Glucose Uptake in Diet-Induced Obese Mice via Activation of GPR120-PI3K/AKT/GLUT4 Pathway," *Biochemical and Biophysical Research Communications* 634 (2022): 189–195, https://doi.org/10.1016/j.bbrc.2022.09.099.

[80] P. Panichayupakaranant, M. Shah, H. Muhammad, Y. Mehmood, R. Khalil, and Z. Ul-Haq, "Superoxide Scavenging and Antiglycation Activity of Rhinacanthins-Rich Extract Obtained from the Leaves of Rhinacanthus Nasutus," *Pharmacognosy Magazine* 13, no. 52 (2017): 652–658, https://doi.org/10.4103/pm.pm_196_17.

[81] A. Riaz, A. Rasul, N. Kanwal, et al., "Germacrone: A Potent Secondary Metabolite with Therapeutic Potential in Metabolic Diseases, Cancer and Viral Infections," *Current Drug Metabolism* 21, no. 14 (2020): 1079–1090, https://doi.org/10.2174/1389200221999200728144801.

[82] S. Sabir, K. Tahir, N. Rashid, S. Naz, B. Masood, and M. A. Shah, "Phytochemical and Antioxidant Studies of Berberis Lycium," *Pakistan journal of pharmaceutical sciences* 26, no. 6 (2013): 1165–1172.